



Final Year Project Report

Modelling Laser-Induced Dynamics in Next Generation Resist Materials for EUVL

Name: Jamie Somers

Student Number: 19330931

Class: AP4

Date: 13/04/2023

Supervisor: Prof. John Costello & Dr. Lazaros Varvarezos

Declaration

Name: Jamie Somers
Student ID Number: 19330931
Programme: AP4
Module Code: PS451
Assignment Title: 4th Year Project Final Report
Submission Date: 11th of April, 2023

I understand that the University regards breaches of academic integrity and plagiarism as grave and serious.

I have read and understood the DCU Academic Integrity and Plagiarism Policy. I accept the penalties that may be imposed should I engage in practice or practices that breach this policy.

I have identified and included the source of all facts, ideas, opinions, viewpoints of others in the assignment references. Direct quotations, paraphrasing, discussion of ideas from books, journal articles, internet sources, module text, or any other source whatsoever are acknowledged and the sources cited are identified in the assignment references.

I declare that this material, which I now submit for assessment, is entirely my own work and has not been taken from the work of others save and to the extent that such work has been cited and acknowledged within the text of my work.

I have used the DCU library referencing guidelines (available at: <http://www.library.dcu.ie/LibraryGuides/Citing&ReferencingGuide/player.html>) and/or the appropriate referencing system recommended in the assignment guidelines and/or programme documentation.

By signing this form or by submitting this material online I confirm that this assignment, or any part of it, has not been previously submitted by me or any other person for assessment on this or any other course of study.

By signing this form or by submitting material for assessment online I confirm that I have read and understood DCU Academic Integrity and Plagiarism Policy (available at: <http://www.dcu.ie/registry/examinations/index.shtml>).

Name:



Date: 11th of April, 2023

Abstract

As technology advances and computer systems become faster and faster, new techniques in computer manufacturing are constantly being implemented in an attempt to keep up with Moore's Law. One of the newest techniques for the production of microprocessors is the use of 13.5 nm light to pattern more transistors on to silicon wafers than was previously possible, this technique is known as extreme-ultraviolet lithography (EUVL) and has been proven effective at producing faster central processing units such as Apple's new M1 & M2 processors. A key component in the patterning of microprocessors is the photoresist which covers the substrate of the wafer and is developed on the areas exposed to laser light to allow patterning to occur. This project explores the modelling of metal coordination complexes which could be viable photoresist candidates in future microprocessor production. Metal coordination complexes are molecules with a central metallic atom (Fe, Ru, Pd etc.) known as the coordination centre that is surrounded by an array of bound molecules known as ligands. Quantum chemistry calculations can be performed in order to simulate the electronic configuration of these molecules and thus extract information related to the excited state structure and dynamics of the molecule in the form of orbital energies, IR & UV/Vis spectra. The calculations will be performed using a suite of quantum chemistry programmes which rely on Hartree-Fock and Density Functional Theory (DFT) which uses an approximated form of the Schrödinger equation and an iterative method to find the minimum energy configurations of the molecules. Our results for both the IR spectroscopy using the Hartree-Fock method and the UV-Vis spectroscopy using Density Functional Theory showed near identical transitions to experimental data found in the literature.

Contents

Abstract	ii
Acknowledgements	vi
1 Introduction	1
1.1 Photoresists for Extreme Ultraviolet Lithography	1
1.2 Inorganic Complexes	3
2 Theory and Background	5
2.1 Schrödinger Equation	5
2.2 Hartree-Fock Method	6
2.2.1 Introduction to Basis Sets	9
2.2.2 Post-Hartree-Fock	10
2.3 Density Functional Theory	10
2.4 Frontier Molecular Orbital Theory	12
2.5 Transition Metals Photophysics	13
3 Experimental Methods	14
3.1 ORCA 5.0.4	14
3.2 Gaussian 16	15
3.3 AOMix 6.88	16
3.4 UV/VIS	16
3.5 IR Spec	16
4 Results, Analysis and Discussion	17
4.1 Solving the Schrödinger Equation for the Hydrogen Atom	17
4.1.1 Separating the angular parts	19
4.1.2 Solving the phi part	19
4.1.3 Solving the theta part	20
4.1.4 Solving the radial part	21
4.1.5 Putting together the full wave function	22
4.2 Using the Hartree-Fock Method to Calculate Water	23
4.3 Using the Hartree-Fock Method to Calculate Benzene	25
4.4 Using Density Functional Theory to Calculate Pyrene	28
4.5 Using Density Functional Theory to Calculate Tris(bipyridine) Ruthenium(II) Chloride	30
5 Conclusion	32
References	34

List of Figures

1	Comparison of the action of the positive and negative photoresists.	2
2	Algorithmic flowchart showcasing the Hartree-Fock Method 2.2	8
3	Algorithmic flowchart showcasing Density Functional Theory 2.3	11
4	Structure of the ORCA input file	14
5	Gaussview 6 Graphical User Interface	15
6	Diagram of a hydrogen atom comprising a single proton and a single electron . .	17
7	Rendered image of a H ₂ O Molecule	23
8	Comparison between H ₂ O IR spectrum and NIST database ^[33]	24
9	Rendered image of a benzene molecule	25
10	Two-electron integrals section of HF output file	25
11	Comparison between C ₆ H ₆ IR Spectrum Hartree-Fock Methods 2.2 and NIST Database	26
12	Rendered image of a pyrene molecule	28
13	Computed Pyrene UV/VIS spectrum compared to the spectrum reported by Thony et al. ^[39]	29
14	Rendered image of a tris(bipyridine) ruthenium(II) chloride molecule	30
15	Computed Tris(bipyridine) Ruthenium(II) Chloride UV/VIS spectrum compared to the spectrum reported by Filevich et al. ^[45]	31

List of Tables

Describing Sigma σ and pi π orbitals	12
The first few associated Legendre polynomials $P_l^{ m_l }(x)$	20
The first few spherical harmonics	21
The first few associated Laguerre polynomials.	22
The complete hydrogenlike atomic wave functions for $n = 1$ and 2	22
Benchmarking results of H_2O using the Hartree-Fock Method 2.2	23
Calculated Vibrational modes of H_2O - comparison With NIST database ^[34]	24
Benchmarking results of C_6H_6 using Hartree-Fock Method 2.2	26
Calculated Vibrational modes of C_6H_6 - comparison With NIST database ^[37]	27
Benchmarking results of $\text{C}_{16}\text{H}_{10}$ using Density Functional Theory 2.3	28
Calculated Vibrational modes of C_6H_6 - comparison With NIST database ^[37]	33

Acknowledgements

Thanks.

1 Introduction

1.1 Photoresists for Extreme Ultraviolet Lithography

The concept of photolithography was first patented all the way back in August of 1855 by french chemist Alphonse Louise Poitevin^[1]. Originally invented as a process to photographically transfer images to a matrix such as plate or stone, it failed to become the industry standard due to its unreliable results^[2] – it didn't take long for photolithography to find its true purpose as a patterning technique for circuits. In 1958 two physicists employed by the U.S military at the National Bureau of Standards presented a paper^[3] at the Professional Group on Electron Devices (PGED) conference in Washington, D.C., which laid the groundwork for the fabrication of transistors using photolithography, this technique was later patented by the two physicists on the 9th of June, 1959^[4].

Today photolithography encompasses a broad range of techniques which are classified according to the wavelength of light used in the process, some examples include ultraviolet photolithography, x-ray photolithography and the focus of this report extreme ultraviolet lithography. Extreme ultraviolet is classified as light spanning wavelengths shorter than the hydrogen Lyman-alpha line^[5] from 120 nm down to 10 nm^[6]. The technique involves the use of a laser-pulsed tin droplet plasma which is reflected onto a photomask which exposes the wafer substrate which is covered in a photoresist. It is this photoresist which coats the substrate that we are exploring potential molecules which we believe could be suitable candidates in future microprocessor production. There are two types of photoresist that can be used to transfer a pattern onto a substrate. The defining characteristic which can be used to group photoresists into one of two categories is whether the exposed light-sensitive photoresist undergoes a chemical process which causes it to dissolve known as a *positive* photoresist, or if the exposed photoresist undergoes a chemical process which causes it to be more stable it is known as a *negative* photoresist. Both of these photoresists are suitable for the lithography process as long as you keep in mind that the positive photoresist will transfer a positive image of whatever mask you are trying to etch on to the substrate, meanwhile the negative photoresist will transfer a negative image of the mask to the substrate. Positive photoresists are the most popular choice for lithography with ultraviolet light sources as they are known to produce a higher resolution pattern transfer^[7].

Extreme Ultraviolet Lithography uses a projection printing method of etching, this means that the pattern present on the mask is scaled down using a system of lenses and the much smaller image of the mask is projected onto the substrate. In order to determine the minimum feature size which can be projection printed onto a substrate such as a silicon wafer the following equation is used:

$$MFS_p = k_1 \frac{\lambda_s}{NA} \quad (1)$$

Where k_1 is an experimentally determined value that depends on the photoresist properties as well as other properties such as processing conditions and the optics used to align the mask. NA is the numerical aperture of the lenses which collimate the light (the closer NA is to 1 the better) and λ_s is the wavelength of source light used in the lithography process.

As manufacturers of microprocessors such as Intel move to these new EUVL machines with the goal of working at 13.5 nm and increasing the lithography resolution meaning a larger number of smaller transistors on a single microprocessor, there is obviously a push to find new photoresist materials with better properties that will reduce the value of k_1 . In this report we will explore materials which we believe have the potential to be new photoresist materials in the EUVL process.

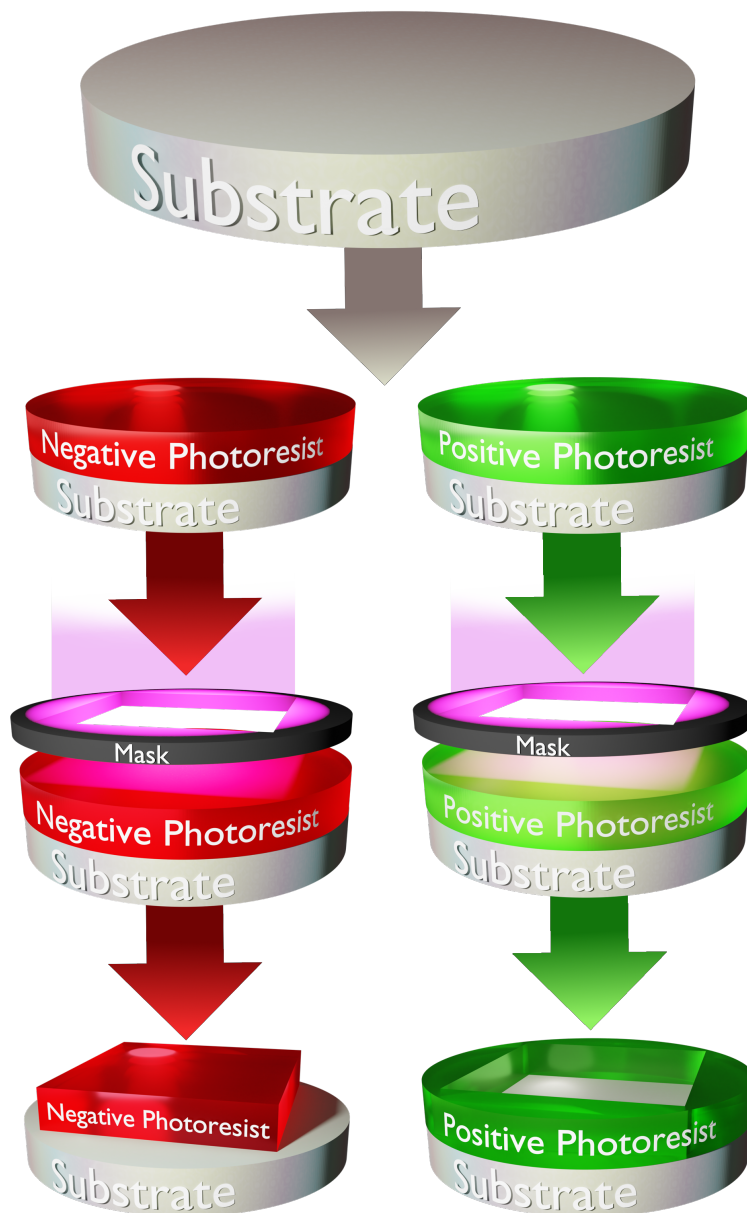


Figure 1: Comparison of the action of the positive and negative photoresists.

In Fig. 1 we see a simplified interpretation of the role photoresists play in the lithographic process and the different results obtained using negative or positive photoresists. We start out with a substrate, in the production of microprocessors this is usually a silicon wafer. A thin uniform layer of photoresist is placed on the substrate using spin coating, the amount of photoresist needed for the entire substrate is poured at the centre of the wafer which is spun at high speed and the centripetal force as well as the surface tension of the liquid work together to create an even coating of the photoresist. Next a mask which contains the pattern you are intending to print onto the substrate is placed above the photoresist and light in the shape of the mask is passed through to the light sensitive material below. In the diagram a simplified large square mask is presented however in practice the masks are typically more intricate with lots of transistor patterns which are projected onto the photoresist using lenses in an effort to make them as small as possible on the surface of the substrate. Finally the chemical process within the photoresist takes affect and you are left with a negative image of the mask or a positive image of the mask depending on the photoresist used. In the diagram we see a square negative photoresist and a circular positive photoresist with a square cutout in the centre.

The viability of a photoresist for use in the microprocessor production process is based on a few key criteria. In order to differentiate clearly between different features on the surface of the substrate, photoresists which can produce higher resolution features are more desirable. Contrast is the difference between the exposed and unexposed parts of the photoresist making the distinction between the two more noticeable, therefore a higher contrast is more desirable. Sensitivity is the minimum energy required to generate clearly identifiable features in a photoresist present on a substrate, theoretically a high sensitivity photoresist is more desirable however it has been noted in the literature that high sensitivity is often accompanied by line roughness^[8]. Line edge is a measurement which comes from the technique by which photoresist performance is measured, the photoresist is exposed in such a way that leaves small thin lines on the surface which is usually imaged using a Critical Dimension Scanning Electron Microscope (CD-SEM) which is a dedicated system for measuring the dimensions of the fine patterns formed on semiconductor wafers^[9]. Some of the other important things to consider when it comes to photoresists are the viscosity of the fluid used, the adhesive strength between photoresist and substrate, the etching resistance of the photoresist and the surface tension of the photoresist which is crucial in the spin coating process which evenly distributes the photoresist across the surface of the substrate.

1.2 Inorganic Complexes

Metals play such a huge role in human history, when we think of periods in history such as the bronze age we are classifying an entire period in human history based on the widespread use of a particular metal. Our ancestors were learning to mix various elements with copper and produce alloys which allowed for the crafting of sharper knives and stronger weapons.^[10] From bronze age to iron age to steel age to gold rushes the impact that metal has had on our advancement as a civilisation can not be understated.

The beginning of chemistry as a field is tied to the fact that gold was an incredibly valuable commodity with the most famous goal of alchemists being the transmutation of common metals into gold.^[11] Although these lofty and ambitious goals were never reached alchemists did make several contributions to a modern-day understand of chemistry. Through the process of exploring "chrysopoeia" (the transmutation of base metals i.e lead into noble metals i.e gold) many meaningful contributions were made such as the discovery of sulfuric acid (H_2SO_4) and hydrochloric acid (HCl) and progress was made on the extraction of metals from ores.^[12] Although a lot of advancements had been made in the name of metallurgy it wasn't until the late nineteenth and early twentieth century where we began exploring the field of coordination chemistry. Early work by Christian Willhelm Blomstrand in 1869 lead to the theory known as complex ion chain theory which was further developed by Danish scientist Sophus Jørgensen and in 1893 following the publications of Alfred Werner^[13] which described complex ion chain theory in the context of chains occurring outside the coordination sphere and binding to the metal occurring within the coordination sphere the accepted version of the theory today was born.

In post-war time such as after World War II many scientific discoveries are made, this was the case for both Crystal Field Theory (CFT) and Ligand Field Theory (LFT) both of these theories would lay the groundwork for Frontier Molecular Orbital Theory which is an essential part of this project that we will discuss in more detail in section 2.4. Both of these theories provide explanations of spectroscopic and structural properties of inorganic coordination compounds. Crystal field theory describes the breaking of degeneracies of electron orbital states such as d and f orbitals due to a static electric field produced by the neighbouring anions. This

theory is crucial in describing various spectroscopies of transition metal coordination complexes. In the 1930s CFT was combined with molecular orbital theory and Ligand Field Theory was born which delivered insights into the chemical bonding processes in transition metal complexes. Out of the two theories Crystal Field Theory is often described as simplistic in its explanation of structures and properties of transition metal complexes, the description of the electrostatics of the metal-ligand interaction are primitive and the theory was built on premises that later turned out to be false such as the assumption that the interaction between metal-ligand is purely electrostatic or the claim that p bonding is not possible despite p bonding being found in many complexes. Despite these pitfalls Crystal Field Theory is still a useful model and can be surprisingly accurate at times when attempting to describe the structure, colour, relative stability or magnetism of metal complexes, many people attribute the simplicity of CFT to be one of its strengths. Meanwhile Ligand Field Theory is considered the more advanced theory rooted in molecular orbital theory but is what it makes up for in accuracy it is hindered by its complexity,

2 Theory and Background

2.1 Schrödinger Equation

The time independent Schrödinger Equation is a linear partial differential equation that describes the exact wave function of a quantum-mechanical system. It can be used to describe the motion of non-interacting electrons like the ones present in an atom, this makes the equation extremely valuable when attempting to understand the electronic structure of atoms and molecules.

The Schrödinger Equation is as follows:

$$\frac{-\hbar^2}{2m}\nabla^2\Psi(r) + V(r)\Psi(r) = E\Psi(r) \quad (2)$$

Where the $\frac{-\hbar^2}{2m}\nabla^2\Psi(r)$ term accounts for the kinetic energy of the system using a Laplace operator with respect to the wave function, the $V(r)\Psi(r)$ term accounts for the potential energy of the system with respect to the wave function and $E\Psi(r)$ is the total energy of the system with respect to the wave function.

It can be written as

$$H\Psi = E\Psi \quad (3)$$

where H is known as the hamiltonian operator.

A wave function (Ψ) is a mathematical function that describes the relationship between the location of an electron at a given point in space in the x, y and z coordinates and the amplitude of its wave which corresponds to its energy. Electrons surrounding the atom are contained within orbitals and it is common for these wave functions to be referred to as orbitals^[14]. An orbital can be thought of as a probability distribution map of where the electron is likely to be found.

Quantum numbers are a method of describing the orbitals and the electrons contained within them in an atom. There are 4 unique quantum numbers for each electron in an atom. The principle quantum number (n) describes the energy of an electron and the most probable distance of the electron from the nucleus. As (n) increases the energy of the orbital decreases and the distance from the nucleus increases, electrons with higher values of (n) are easier to remove from an atom. The orbital angular momentum (l) describes the shape of the orbital, the value of (l) is dependent on the value of (n) and can range from 1 to (n) - 1. Each orbital sub shell is associate with an (l) value, (l) = 0 is known as an s-orbital and is spherical in shape, (l) = 1 is known as a p-orbital and has an infinity symbol shape, (l) = 2 is known as a d-orbital and has a four leaf clover shape and (l) = 3 is known as an f-orbital and has a tetrahedral shape. The magnetic quantum number (m_l) specifies the orientation in space of an orbital with a specific value of (n) and (l). The value of m_l ranges from -(l) to +(l). This divides up the sub shells further i.e an s-orbital is symmetrical (l) = 0 and therefore only has one orientation (m_l) = 0 however a p-orbital (l) = 1 now has a p_x , p_y and p_z configuration ($m_l = -1,0,1$). The fourth and final quantum number is known as the spin quantum number (m_s). It describes the spin of an electron around an axis with both angular momentum and orbital angular momentum, angular momentum is a vector so the spin quantum number has both a magnitude 1/2 and a direction (+ or -).

Throughout this report we will refer back to these quantum numbers to describe the orbitals of the molecules we are discussing and explain their relevance. The spin quantum number (m_s) will become particularly important when discussing the triplet state of one of our molecules.

2.2 Hartree-Fock Method

In 1927, one year after the discovery of the Schrodinger Equation, Douglas Reynier Hartree introduced a procedure to calculate approximate wave functions and energies for atoms and ions^[15]. Foregoing the use of empirical parameters, Hartree wanted a method of solving the many-body time-independent Schrodinger Equation from fundamental physical principles (*ab initio* meaning "from first principles" or "from the beginning").

Originally Douglas Hartree proposed a method of solution known as the Hartree product, which calculated the solutions to the Schrodinger Equation for individual electrons in each state. The assumption being that the product of the solutions should at least approximate a solution, this simple method of combining wave functions of individual electrons is known as the Hartree product

$$\Psi(x_1, x_2, x_3, \dots, x_N) = \psi_\alpha(x_1)\psi_\beta(x_2)\psi_\gamma(x_3)\dots\psi_\pi(x_N) \quad (4)$$

In 1930, both J.C Slater^[16] and V. A. Fock^[17] independently pointed out that the Hartree product did not respect the principle of antisymmetry of the wave function. The solution to this problem was to use a Slater determinant, a determinant of one-particle orbitals was first used by both Heisenberg^[18] and Dirac^[19] independently in 1926. To this day the original Hartree product is considered to be an approximation of the Hartree-Fock method by neglecting exchange.

$$\Psi(x_1, x_2, x_3, \dots, x_N) = \frac{1}{\sqrt{N!}} \begin{vmatrix} \chi_1(x_1) & \chi_2(x_1) & \dots & \chi_N(x_1) \\ \chi_1(x_2) & \chi_2(x_2) & \dots & \chi_N(x_2) \\ \vdots & \vdots & \ddots & \vdots \\ \chi_1(x_N) & \chi_2(x_N) & \dots & \chi_N(x_N) \end{vmatrix} \quad (5)$$

If we take the simple example of a 4x4 determinant we can clearly show that the principle of antisymmetry of the wave function is respected.

$$\Psi(x_1, x_2) = \frac{1}{\sqrt{2!}} \begin{vmatrix} \chi_1(x_1) & \chi_2(x_1) \\ \chi_1(x_2) & \chi_2(x_2) \end{vmatrix} \quad (6)$$

$$\Psi(x_1, x_2) = \chi_1(x_1)\chi_2(x_2) - \chi_1(x_2)\chi_2(x_1) \quad (7)$$

Here it is clearly shown that when there is an exchange of two fermions x_1 and x_2 there is also a change in sign thus, the use of Slater determinants ensures conformity to the Pauli exclusion principle.

The Hartree-Fock method is used to solve the time-independent Schrodinger equation for multi-electron atoms or molecules as described in the Born-Oppenheimer approximation. There is no known analytical solutions for many electron systems (however we will explore the analytical solution for a one-electron hydrogen atom later in the report) the problem is solved numerically. The Hartree-Fock approximation involves solving nonlinear equations through iteration; this iteration process is known as an SCF method or "self-consistent field method".

Other than the Born-Oppenheimer approximation: treating the nuclei in the system as fixed due to the larger relative mass of the nucleus compared to the electron meaning their motions happen on completely different time scales. The Hartree-Fock method also describes each energy eigenfunction as a single Slater determinant and neglects electron correlation terms such as Coulomb correlation.

The connection between the Hartree-Fock method and the variational principle comes about in the energy expectation value $\langle \Psi | H | \Psi \rangle$ of a Slater determinant state Ψ . According to quantum mechanics, the hamiltonian operator H for a many-body system composed of several nuclei and electrons is:

$$H_{elec} = \underbrace{-\sum_{i=1}^N \frac{1}{2} \nabla_i^2}_{\text{Electrons' kinetic energy}} \quad \overbrace{-\sum_{i=1}^N \sum_{A=1}^M \frac{Z_A}{r_{iA}}}_{\text{Coulomb attraction between electrons and nuclei}} \quad + \underbrace{\sum_{i=1}^N \sum_{j>i}^N \frac{1}{r_{ij}}}_{\text{Repulsion between electrons}} \quad (8)$$

In order to use the hamiltonian to solve the electronic Schrodinger Equation, we will need to break down the equations into a set of one-electron equations. The first term is the sum of single electron kinetic energies and the second term is the sum of attractions between each electron and all nuclei, these two terms are separable. The last term is the sum of repulsion between all electron-pairs and is not divisible into single electron terms, this is where one of the Hartree approximations is used to approximate the electron-electron repulsion averagely. Instead of calculating the repulsion between all electron pairs, we instead calculate the repulsion between each electron and the average field of all other electrons in the system. This allows us to write the Hamiltonian as a sum of one-electron operators:

$$H_{elec} = \sum_{i=1}^N f(x_i), \quad f(x_i) = -\frac{1}{2} \nabla_i^2 - \sum_{A=1}^M \frac{Z_A}{r_{iA}} + v^{HF}(x_i) \quad (9)$$

Where v^{HF} is the average potential that each electron experiences because of all the other electrons in the system, $f(x)$ is a one-electron operator known as the Fock operator.

$$f(x_i)\chi(x_i) = \epsilon\chi(x_i) \quad (10)$$

Although this is now a one-electron problem, the Hartree-Fock potential v^{HF} depends on the entire system's wave function and makes the problem nonlinear. It is this nonlinearity that requires the problem to be solved iteratively. Eq.10 initially seems counter-intuitive as you can't find the wave function $\chi(x_i)$ without first knowing the wave function $\chi(x_i)$. The basic concept of the Hartree-Fock method is that using an initial trial wave function, the average field is calculated, then the eigenvalue equation is solved using this average field and this process is repeated iteratively until some convergence criteria $\leq \epsilon$ is satisfied – this is the self consistent part of the method.

Despite the approximation of the repulsion term as the repulsion between a single electron and the average of all the other electrons in the system the computation of two-electron repulsion integrals is almost always the most expensive step of integral-direct self consistent field methods^[20]. Formally it scales as $O(N^4)$ ^[21], where N is the number of electrons or the number of Gaussian basis functions used to represent the molecular wave function.

We will see later on in the report just how big the number of two-electron repulsion integrals gets when attempting to use the Hartree-Fock method for relatively large molecules such as benzene which contains 42 electrons, this complexity along with the growing determinant size (benzene has a 42 x 42 slater determinant) introduces the problem that Hartree-Fock becomes untenable as a useful method of carrying out quantum chemistry calculations for extremely large molecules such as the inorganic complexes we are considering as potential photoresist materials.

A good method of visualising the processes carried out as part of the Hartree-Fock method is in the form of an algorithmic flowchart

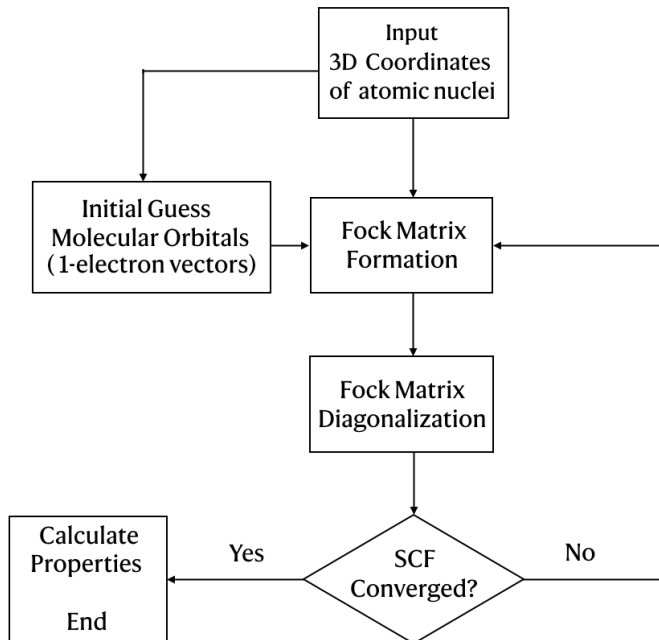


Figure 2: Algorithmic flowchart showcasing the Hartree-Fock Method 2.2

The method begins by Inputting the 3D coordinates of the atomic nuclei you would like to perform the calculation on. The Initial Guess Molecular Orbitals (1-electron vectors) is the part we have previously discussed about using an initial trial wave function. The Fock matrix is defined by the Fock operator and is described as

$$\hat{F}(i) = \hat{h}(i) + \sum_{j=1}^{n/2} [2\hat{J}_j(i) - \hat{K}_j(i)] \quad (11)$$

where $\hat{F}(i)$ is the Fock operator for the i -th electron, $\hat{h}(i)$ is the one-electron Hamiltonian for the i -th electron both of which we have discussed previously. n is the number of electrons and $\frac{n}{2}$ is the number of occupied orbitals in the closed-shell system, $\hat{J}_j(i)$ is the Coulomb operator, defining the repulsive force between the j -th and i -th electrons in the system and $\hat{K}_j(i)$ is the exchange operator, defining the quantum effect produced by exchanging two electrons. Again because the Fock operator is a one-electron operator, it does not include the electron correlation energy.

Finally the constructed Fock matrix is diagonalised and eigenvalues and eigenvectors are obtained. It is determined whether the self consistent field method converges to or below some predetermined value and the properties of the system can be calculated or if the iterative process needs to be repeated with the final wave function acting as an initial trial wave function.

2.2.1 Introduction to Basis Sets

One of the downsides of Hartree-Fock equations is that they are difficult to solve in real coordinate space. A major advancement for the Hartree-Fock method came in 1951 when C.C.J Roothaan demonstrated that by introducing a set of known spatial *basis functions*^[22], the difficult differential Hartree-Fock equations could be reformulated as an algebraic equation which could be solved by standard matrix techniques. We can approximate the i -th spatial wave function by a linear combination

$$\psi_i = \sum_{\mu=1}^K C_{\mu i} \phi_{\mu} \quad i = 1, 2, \dots, (K \geq \frac{N}{2}) \quad (12)$$

Where ϕ_{μ} represents a set of basis functions for the space of square integrable functions^[23].

Slater orbitals laid the groundwork for the Hartree-Fock method and were the main method of calculation for many years, however they are no longer directly used in the calculation because the integrals in the resulting secular determinants are difficult to evaluate. The integrals involving more than one nuclear center, known as *multicenter integrals* are particularly difficult to calculate using Slater orbitals. The use of Gaussian functions was adopted as a replacement for Slater orbitals which made calculating all these multicenter integrals very easy^[24].

For this method to work we need to work with Gaussian-type orbitals of the form

$$G_{nlm}(r, \theta, \phi) = N_n r^{n-1} e^{-\alpha r^2} Y_l^m(\theta, \phi) \quad (13)$$

A common basis set in quantum chemistry calculations is known as the STO-3G basis set. This basis set gets its name from the fact that the Slater orbital (STO) is being represented by the sum of three Gaussian functions. There are many different variations of this basis set however they all follow the same naming convention i.e STO-1G uses one Gaussian function, STO-2G uses two Gaussian functions etc.

The atomic orbitals in the basis set are now expressed as a sum of Gaussian functions so that the wave function of the i -th electron is

$$\psi_i = \sum_{k=1}^M c_{ki} \phi_k \quad (14)$$

Where ϕ_k is the atomic orbital, M is the number of atomic orbitals used to construct the molecular orbitals and c_{ki} is a value determined to minimise the energy of the molecule.

Throughout this report multiple references will be made to the basis set LANL2DZ (Los Alamos National Laboratory 2 double- ζ). These types of basis sets consist of functions that can adjust the shape of the atomic orbital by expressing each atomic orbital as a sum of two Slater-type orbitals that differ only in the value of their exponent ζ . Basis sets generated from the sum of two Slater orbitals with different orbital exponents are called *double-zeta basis sets*

A linear combination of two Slater orbitals of the same type but with different orbital exponents ζ_1 and ζ_2 allows us to generate an atomic orbital of adjustable size by varying a constant d where the orbital is written as

$$\phi(r) = \phi^{STO}(r, \zeta_1) + d\phi^{STO}(r, \zeta_2) \quad (15)$$

Where ζ_1 is the smaller orbital exponent and ζ_2 is the larger orbital exponent.

2.2.2 Post-Hartree-Fock

Subsequent methods of improving on the Hartree-Fock method were devised, one of the most notable improvements being the inclusion of electron correlation which is a more accurate method of including the repulsion which exists between electrons compared to the original Hartree-Fock method where repulsion was averaged.

Usually, post-Hartree-Fock methods give more accurate results than Hartree-Fock calculations, however this added accuracy comes with the price of added computational cost. Like with a lot of quantum chemistry, post-Hartree-Fock has been developed over multiple years and thus there are many different sub-methods to choose from within the post-Hartree-Fock umbrella including Configuration interaction (CI)^[25], Coupled cluster (CC)^[26] and Multi-configuration time-dependent Hartree (MCTDH)^[27] to name a few.

2.3 Density Functional Theory

Density Functional Theory would come as a paradigm shift to the world of quantum chemistry; its low computational cost combined with useful accuracy has made DFT a standard technique in most branches of chemistry and materials science^[28]. In 1964 the Hohenberg-Kohn (HK) theorem opened up the possibility for an exact method of finding the electronic structure of atoms based on ground state electron density $\rho(r)$.

The Hohenberg-Kohn theorem^[29] stated that for non-degenerate ground states,

1. The ground state electron density $\rho(r)$ of a system of interacting electrons uniquely determines the external potential $v(r)$ in which the electrons move and thus the Hamiltonian and all physical properties of the system.
2. The ground-state energy E_0 and the ground-state density $\rho_0(r)$ of a system characterized by the potential $v_0(r)$ can be obtained from a variational principle which involves only the density, that is, the ground-state energy can be written as a functional of the density, $E_{v_0}[n]$, which gives the ground-state energy E_0 if and only if the true ground-state density $\rho_0(r)$ is inserted. For all other densities $\rho(r)$, the inequality

$$E_0 = E_{v_0}[\rho_0] < E_{v_0}[n]$$

3. There exists a function $F[n]$ such that the energy functional can be written as

$$E_{v_0}[n] = F[n] + \int d^3r v_0(r)n(r)$$

The modern version of Density Functional Theory that we think of today is known as Kohn-Sham DFT which follows the basic principle of defining self-consistent equations which must be solved for a set of orbitals given an initial density $\rho(r)$ which is exactly equal to the real system.

As with the Hartree-Fock method, the easiest way to visualise the processes carried out as part of Kohn-Sham Density Functional Theory is in the form of an algorithmic flowchart. One substitution we made to the Kohn-Sham Density Functional Theory is our choice of functional, throughout the report I will reference a B3LYP 'Hybrid Functional' which are a set of functions that represent the electronic wave function, we choose to use B3LYP because it includes a term for exchange interaction and is widely used in the literature making it easier to compare our results to literature values.

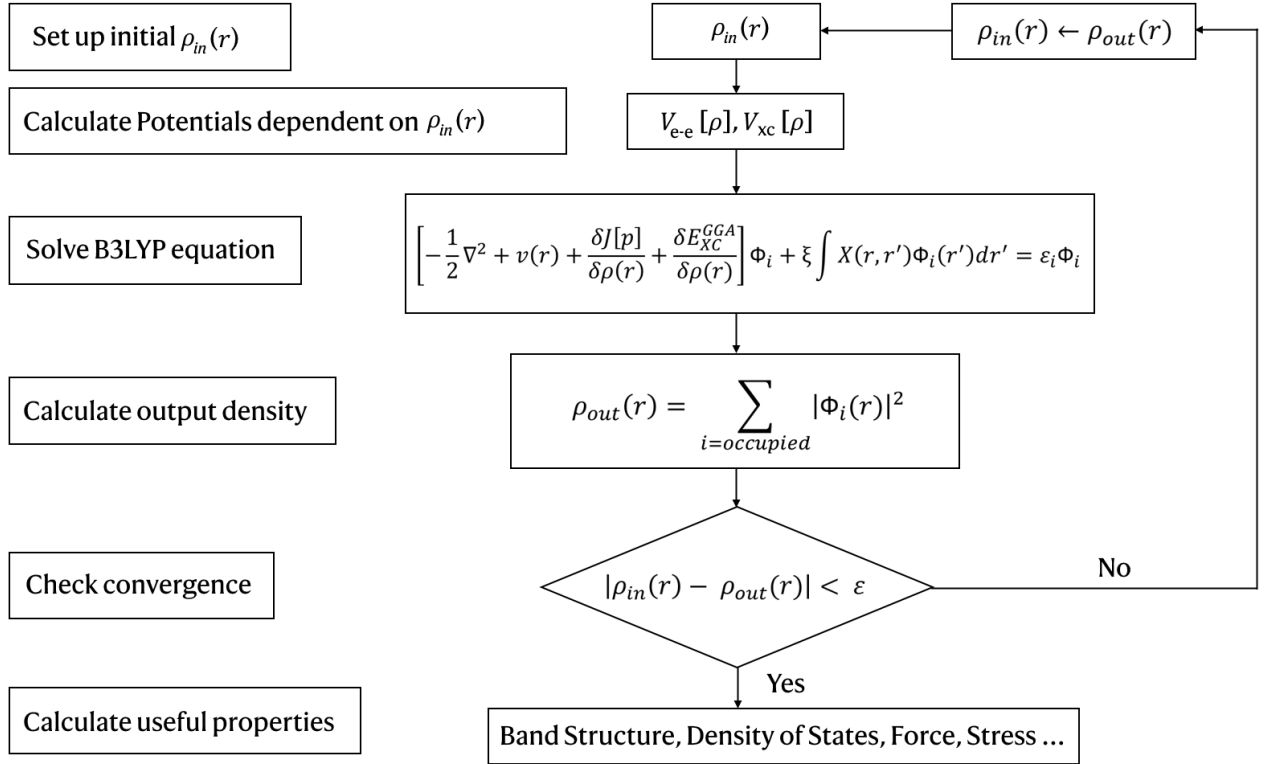


Figure 3: Algorithmic flowchart showcasing Density Functional Theory 2.3

Density Functional Theory involves the use of an initial density $\rho(r)$, compared to the many-body electronic wavefunction which is a function of $3N$ variables (where N is all electrons in the system). Despite its apparent simplicity, the Hohenberg-Kohn theorems assure us that this value will be able to determine all ground-state properties of the system with the total ground state energy being a functional of the density. Although we are not starting with a ground state wave function in principle the relationship that exists between the ground state density and the ground state wave function which is a unique functional of the ground state density can ultimately be used to get a wavefunction.

We then calculate potentials dependent on the initial density such as the electron-electron Coulomb repulsion $V_{e-e}[\rho]$ and the exchange-correlation potential $V_{xc}[\rho]$. All of these terms feed into what is often referred to as the Kohn-Sham Equations, however in our case the Kohn-Sham Equations have been altered slightly based on our chosen functional B3LYP. B3LYP is a 'hybrid' functional meaning it contains some exact exchange, it introduces some semi-empirical parameters based on the Becke-determined B3P91 functional. Our B3LYP equation has the standard terms found in a typical Kohn-Sham equation such as the kinetic-energy operator $-\frac{1}{2}\nabla^2$ and the electron-electron interaction and the exchange interaction $\frac{\delta J[\rho]}{\delta\rho(r)}$ and $\frac{\delta E_{xc}^{GGA}}{\delta\rho(r)}$ which are referred to as universal functionals. Meanwhile the rest of the terms are known as the external potential and are considered a non-universal functional, as it depends on the system under study.

Once the Kohn-Sham like equation has been calculated it yields a Kohn-Sham orbital Φ_i , we can take the absolute value squared of this Kohn-Sham orbital and sum over the total number of electrons in the system to arrive back at a reproduced density $\rho_{out}(r)$ of the original many

body system. We then get the magnitude of the original inputted density $\rho_{in}(r)$ minus the reproduced density $\rho_{out}(r)$ in an effort to get the total energy below some predetermined value ϵ . This is where the self consistent part of the method comes in as if the total energy is not below the predetermined value the output density $\rho_{out}(r)$ is now used as the initial density of the system and the process is repeated with the goal of getting a total energy value below ϵ .

Density Functional Theory (and the Hartree-Fock Method) output files contain some immediately useful values for the purposes of characterising molecules and their molecular dynamics such as vibrational frequencies which can be used to generate IR spectra clearly delineating the bending and stretching modes of molecules such as H₂O. If however, our goal is to produce more characterisation data which will give information related to the absorption of energy within the molecule with hopes of characterising transitions we will first need to explore Molecular Orbital Theory.

2.4 Frontier Molecular Orbital Theory

Frontier Molecular Orbital Theory (FMOT) builds on the previous understanding of Ligand field theory that bonding Molecular Orbitals (MOs) primarily possess ligand characteristics and the anti-bonding MOs are primarily localised in the metal, this means that metals are electrophilic with many unfilled MOs meanwhile the ligands are nucleophilic with many filled MOs.

In order to understand FMOT we have to focus on orbitals which are at the frontier of electron occupation, one ones which contain the highest-energy occupied orbitals and the lowest-energy unoccupied orbitals (HOMO and LUMO). We view the HOMO as being nucleophilic or electron donating while the LUMO is electrophilic or electron accepting. We can use labels to describe these different types of orbitals and the way they behave towards electrons.

TABLE 1

Describing Sigma σ and pi π orbitals

Orbitals	Frontier Molecular Orbitals	Typical Electronic Behaviour
π -acceptor	Low-lying π^*	Electron accepting
π -donor	High-lying π	Electron donating
σ -acceptor	Low-lying σ^*	Electron accepting
σ -donor	High-lying σ^*	Electron donating

We can use these descriptions to try and label the transitions we see between our metal centred complex and the ligands surrounding it. We know that upon visible light irradiation, Ru-based complexes display low energy metal-to-ligand charge transfer (¹MLCT) transitions. This is because an electron is being excited from the ruthenium metal centres d subshell π based HOMO to the ligands π^* based LUMO.^[30] We also know that this ¹MLCT excited state experiences rapid intersystem crossing to the ³MLCT excited state which we will explore further in the next section.

2.5 Transition Metals Photophysics

The UV-Visible spectrum for Transition Metals was first explored back in the 1950s around the same time as the development of Ligand Field Theory. Transition metal complexes possess unique chemical and spectroscopical properties and are used in a variety of photochemical devices like solar cells thanks to the continued study and evolution of research around quantum yields, luminescence lifetimes and electron transfer.

There are five main types of electronic transitions which occur within transition metals:

- (i) Metal-centered (MC) transition, these excitations of electrons occur within the confines of the metal complex. They are in principal forbidden by Laporte rules in centrosymmetric environments however they are partially allowed as a result of vibronic and spin-orbit coupling. This results in the transition being much lower in energy compared to charge-transfer transitions.
- (ii) Ligand-to-Metal Charge Transfer (LMCT) transitions. Involve the promotion of electrons from occupied ligand orbitals to the partially empty d shell of the metal.
- (iii) Metal-to-Ligand Charge Transfer (MLCT) transitions. These transitions are excitations of electrons from metal d-based orbitals to low-lying empty orbitals located at the ligands, typically t_{2g} to π^* .
- (iv) Ligand Centred (LC) transitions involve the promotion of electrons within the orbitals of the same ligand, typically π to π^* .
- (v) Ligand-to-Ligand Charge Transfer (LLCT) transition, involves movement of electrons to orbitals located on different ligands.

In principle, following the selection rules of UV-Vis spectroscopy would lead you to understand that transitions between states of different multiplicity are strictly forbidden. Despite this rule we still see InterSystem Crossing (ISC) which is a radiation-less process involving a transition between two electronic states with different spin multiplicity.

Transition metals such as Ru(II) contain a high atomic number d^6 metal centres and favour intersystem crossing after undergoing Metal-to-Ligand Charge Transfer, this is due to their more intense spin-orbit coupling^[31].

We know from the Pauli exclusion principle that a pair of electrons in the same energy level must have opposite spins. In singlet states all electron spins are paired, so an excited electron is still paired with the ground state electron. In a triplet state the excited state electron is no longer paired and the unpaired excited state electron and ground state electron have parallel spin. Since we will be working with a metal complex containing Ru(II) at its core this will be essential in understanding the MLCT transition.

3 Experimental Methods

3.1 ORCA 5.0.4

Orca is an *ab initio* quantum chemistry program that allows for the calculation of electronic structures using state of the art methods such as density functional theory, many-body perturbation, coupled cluster, multi reference methods and semi-empirical quantum chemistry methods.

It was designed and developed in the Neese Research Group under Frank Neese who is a German theoretical chemist at the Max Planck Institute of Coal Research and is the lead author of the computer program. The program was based on one Neese had written as part of his PhD thesis back in 1995^[32] and was officially released to the public in 2011 alongside an article published in WIREs Computational Molecular Science. Since its release it has seen continuous growth as a reliable source in academic papers, as of 2023 ORCA has received almost 10,000 citations according to Scite.ai.

For the purposes of this project we initial started with ORCA 5.0.4 as it was free for academics and was well known within the quantum chemistry community, we used the program to perform geometry optimisation on small diatomic molecules such as H_2 , HF and NO as well as slightly larger molecules like H_2O and C_6H_6 . We also performed all of the Hartree-Fock measurements through ORCA to collect our IR spectra and vibrational modes to compare with experimental results found in the literature. Although ORCA is a commercial software available for purchase it is mostly used within the realm of academia as a free software and as a result is missing some of the quality of life features you would expect to see in a predominantly commercial software package sold to companies such as a Graphical User Interface (GUI). ORCA is installed directly to the command line and all interactions with the software are done through an input file which contains the coordinates of your molecule and the instructions on what calculation you are trying to perform, or through specific commands included when running the input file in the command line. Everything that comes after the "!" in an ORCA input file is

```
!HF DEF2-SVP
%SCF
  MAXITER 500
END
* xyz 0 1
O  0.0000  0.0000  0.0626
H -0.7920  0.0000 -0.4973
H  0.7920  0.0000 -0.4973
*
```

Figure 4: Structure of the ORCA input file

considered the main input, In this example a Hartree-Fock calculation is being ran denoted by the HF input with a DEF2-SVP basis set, the "%" is used to denote specific options, here the user is telling ORCA to try and solve the Self-Consistent Field Method with a max iteration number of 500, if it does not converge within that number of iterations the calculation will be terminated. "END" denotes the end of the main input and "*" is the beginning of the structure section which contains the geometric coordinates of the molecule with an x, y and z value. 0 and 1 denote the system's charge and multiplicity respectively. Running the input file in the command line using the ORCA command will result in the creation of an output file in the same folder as the input file with the results of the Hartree-Fock Method.

3.2 Gaussian 16

Gaussian is a general purpose computational chemistry package, the program was originally widely distributed to quantum chemists through the Quantum Chemistry Program Exchange however in 1987 it was developed and licensed by Gaussian, Inc. and has remained that way ever since.

Compared to ORCA, Gaussian has a much more user friendly interface and is clearly targeted toward a commercial demographic who are willing to pay for software with an improved user experience and a much more personal and direct form of customer support. Despite using Gaussian 16 to perform all of the Density Functional Theory calculations included in the results section of this report, Gaussian 16 was never actually installed on a local machine. The graphical interface Gaussview 6 was installed which allows the user to create a Gaussian input file for any molecule by building the desired molecule in a 3-dimensional viewport and saving the input file with the desired calculations to be performed. Once the Gaussian 16 input files

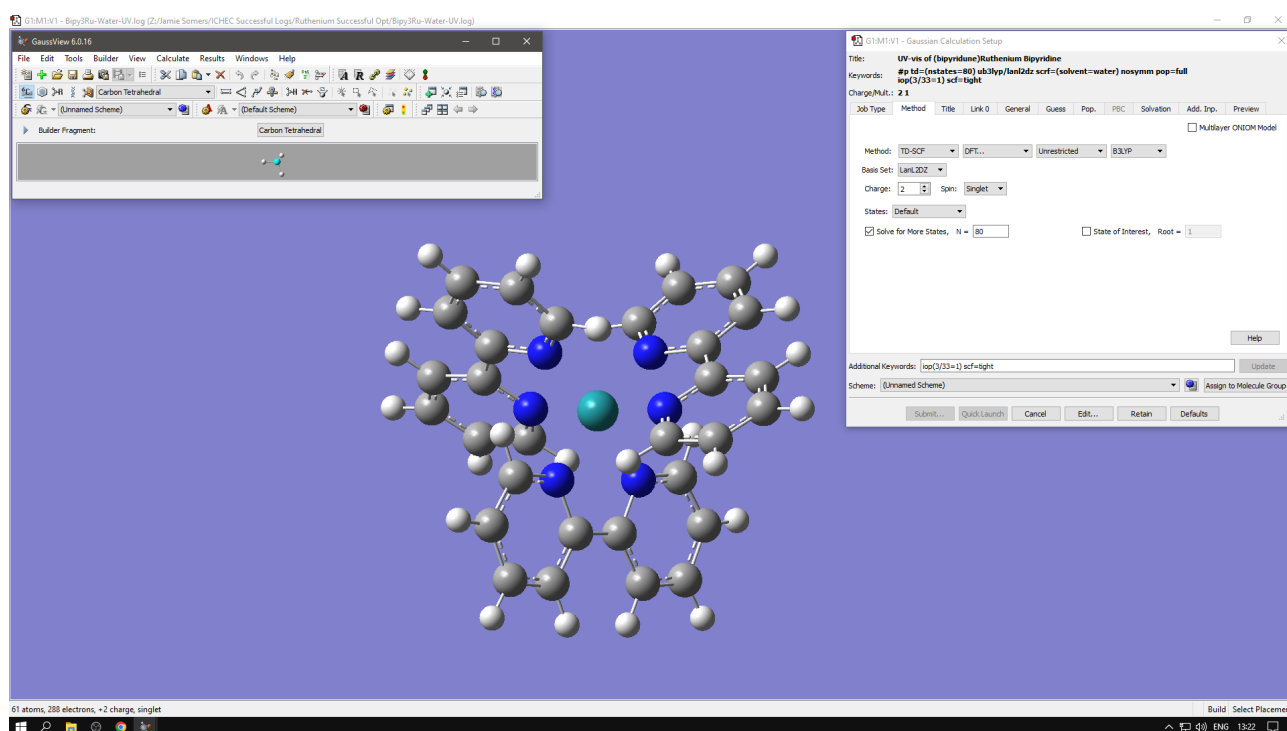


Figure 5: Gaussview 6 Graphical User Interface

were created a corresponding bash script was made and both files were uploaded to the KAY supercomputer at the Irish Centre for High-End Computing (ICHEC). Gaussview allows you to create jobs with multiple different methods such as Ground State or Time-Dependent Self Consistent Field which can be performed alongside multiple different methods such as Hartree-Fock, Semi-empirical, Density Functional Theory and many more. You can change the spin to be default spin, restricted, unrestricted or restricted-open. You can change the functional to 12 included options and the basis set comes with 16 options to choose from and the ability to input a custom basis set not listed. The ability to enter the charge of the molecule manually will affect the available spin options for the given molecule. You can also choose which states to target such as singlet-only, triplet-only or leave the default states as well as the exact number of states you want to solve for. Gaussview also allows you to choose from a wide range of solutions to place your molecule into for UV/VIS measurements, this is extremely important when comparing results with non-gas phase spectra found in the literature. Once the Gaussian job is finished running a .log file is produced with all of the data from the calculation.

3.3 AOMix 6.88

AOMix is described as a user-friendly software to perform molecular orbital (MO) analysis. The purpose of AOMix is to read in the .log file produced by Gaussian which contains crucial information about the electronic structure of the molecule such as its wave function and energy and to output an interpretable file containing information to describe the electronic structure, this comes in the form of a text file labelled "UV-Vis-spectrum" which contains both the wavenumber cm^{-1} and wavelength nm ranges for the x-axis and the molar absorbance of the molecule for the y-axis. The UV-Vis spectrum can be set up to fit either a Gaussian curve function $G(x)$ or a Lorentzian curve $L(x)$ but by default it is set to a pseudo-Voigt function. This is a convolution of both a Cauchy-Lorentz distribution and a Gaussian distribution which can be weighted one way or the other using a fourth parameter η which has a value between 0 and 1. The pseudo-Voigt function is as follows:

$$pV(x) = \eta G(x) + (1 - \eta)L(x) \quad (16)$$

The software also produces a text file called "UV-Vis-transitions" which contains both the wavenumber cm^{-1} and wavelength nm range as well as the oscillator strength at any given value which can be graphed to obtain a line graph denoted exactly where each transition is located on the spectrum as well as the percentage contribution of the excitation.

3.4 UV/VIS

Ultraviolet-Visible Spectroscopy is a characterisation technique used to obtain the absorbance spectra for a given solid or liquid compound. The absorbance of light excites the electrons from their ground state to their first singlet excited state and the wavelength at which the absorption takes place gives us information about how much energy was needed for the excitation to take place with shorter wavelengths of light carrying more energy and longer wavelengths carrying less energy. For the purposes of this experiment we will excite molecules using a wavelength range of 200 nm to 800 nm and attempt to label the transitions based on the peaks in absorption obtained from the UV-VIS Spectrum. The principle behind UV-Vis Spectroscopy is the Beer-Lambert Law which states that for a single wavelength the absorbance (A) is equal to the molar absorptivity of the molecule (ϵ) multiplied by the path length (b) and the concentration of the solution (c). The equation is as follows

$$A = \epsilon bc \quad (17)$$

For all of the UV-Vis Spectra shown in this report the data will be graphed using the molar absorptivity (ϵ) as a function of wavelength (nm).

3.5 IR Spec

Infrared Spectroscopy uses the idea that molecules will absorb frequencies that are characteristic of their structure, the frequencies that match the vibrational frequency of the molecules will be absorbed. In order for a vibrational mode to be "IR active" it needs to have a change in the dipole moment. We will use these IR active resonant frequencies to label the symmetric and asymmetric oscillations of molecules and compare these with agreed upon experimental values found in the NIST database.

4 Results, Analysis and Discussion

4.1 Solving the Schrödinger Equation for the Hydrogen Atom

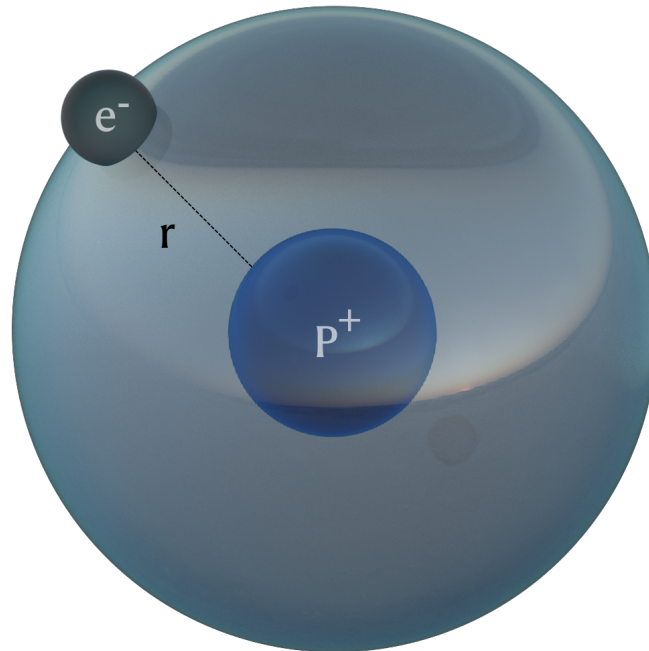


Figure 6: Diagram of a hydrogen atom comprising a single proton and a single electron

Atomic hydrogen is an electrically neutral atom containing a single positively charged proton and a single negatively charged electron (denoted by P^+ and e^- respectively in Fig. 6). In this simplified (Bohr model) picture of the atom, the electron is bound to the nucleus by the Coulomb force, the two subatomic particles are separated by a distance r . Hydrogen is considered the simplest element on the periodic table, with a ground state that has quantum numbers $n=1$, $l = 0$, $m_l = 0$ and $m_s = \pm\frac{1}{2}$ where the sole electron occupies this 1s orbital. It is this simplicity that makes the hydrogen atom of special significance in quantum mechanics, as a simple two-body problem that makes it the only system for which the Schrödinger equation can be solved analytically.

We will prove that the Schrödinger Equation can be solved analytically for hydrogen by way of a direct proof. The solution to the Schrödinger Equation for Hydrogen is as follows.

We will start by assuming the proton in our diagram P^+ is fixed at the origin and the electron e^- is interacting with the proton through a Coulombic potential denoted by:

$$V(r) = -\frac{e^2}{4\pi\epsilon_0 r} \quad (18)$$

where e is the elementary charge of the proton (1.602×10^{-19} C), ϵ_0 is the vacuum permittivity ($8.854187817 \times 10^{-12}$ F \cdot m $^{-1}$) and r is the distance between the electron and the proton. The factor $4\pi\epsilon_0$ arises as a result of using SI units, and the spherical geometry means we should be using a spherical coordinate system with a proton as our origin.

The Hamiltonian operator for a hydrogen atom is

$$\hat{H} = -\frac{\hbar^2}{2m_e} \nabla^2 - \frac{e^2}{4\pi\epsilon_0 r} \quad (19)$$

We have discussed the components of the Hamiltonian operator previously however we will need to go into more detail about the different variables for the purpose of this solution, starting with the Laplacian ∇^2 . The Laplace operator is a second-order differential operator in the n -dimensional Euclidean space, defined as the divergence of the gradient. The Laplace operator for spherical coordinates is as follows

$$\nabla^2 = \frac{1}{r^2} \frac{\partial}{\partial r} \left(r^2 \frac{\partial}{\partial r} \right) + \frac{1}{r^2 \sin \theta} \frac{\partial}{\partial \theta} \left(\sin \theta \frac{\partial}{\partial \theta} \right) + \frac{1}{r^2 \sin^2 \theta} \frac{\partial^2}{\partial \phi^2} \quad (20)$$

Making these substitutions into Eq.2 which we introduced when discussing the Schrödinger Equation previously we get

$$-\frac{\hbar^2}{2m_e} \left[\frac{1}{r^2} \frac{\partial}{\partial r} \left(r^2 \frac{\partial \psi}{\partial r} \right) + \frac{1}{r^2 \sin \theta} \frac{\partial}{\partial \theta} \left(\sin \theta \frac{\partial \psi}{\partial \theta} \right) + \frac{1}{r^2 \sin^2 \theta} \frac{\partial^2 \psi}{\partial \phi^2} \right] - \frac{e^2}{4\pi\epsilon_0 r} \psi(r, \theta, \phi) = E \psi(r, \theta, \phi) \quad (21)$$

We can simplify our equation by multiplying by $2m_e r^2$

$$-\hbar^2 \left(\frac{\partial}{\partial r} r^2 \frac{\partial \psi}{\partial r} \right) - \hbar^2 \left[\frac{1}{\sin \theta} \left(\frac{\partial}{\partial \theta} \sin \theta \frac{\partial \psi}{\partial \theta} \right) + \frac{1}{\sin^2 \theta} \frac{\partial^2 \psi}{\partial \phi^2} \right] - 2m_e r^2 \left[\frac{e^2}{4\pi\epsilon_0 r} + E \right] \psi(r, \theta, \phi) = 0 \quad (22)$$

The θ and ϕ dependent terms are restricted to the first square bracket of the equation, this implies the use of separation of variables to separate our distance from the origin r from the two angles θ and ϕ in the form

$$\psi(r, \theta, \phi) = R(r)Y(\theta, \phi) \quad (23)$$

where R is the radial component and Y is the angular component.

Since $R = R(r)$ and $Y = Y(\theta, \phi)$ the partial derivatives become regular derivatives.

$$\underbrace{-\frac{\hbar^2}{R(r)} \left[\frac{d}{dr} \left(r^2 \frac{dR}{dr} \right) + \frac{2m_e r^2}{\hbar^2} \left(\frac{e^2}{4\pi\epsilon_0 r} + E \right) R(r) \right]}_{\text{Radial Component}} - \underbrace{\frac{\hbar^2}{Y(\theta, \phi)} \left[\frac{1}{\sin \theta} \frac{\partial}{\partial \theta} \left(\sin \theta \frac{\partial Y}{\partial \theta} \right) + \frac{1}{\sin^2 \theta} \frac{\partial^2 Y}{\partial \phi^2} \right]}_{\text{Angular Component}} = 0 \quad (24)$$

Because r , θ , and ϕ are independent variables, we may write

$$-\frac{1}{R(r)} \left[\frac{d}{dr} \left(r^2 \frac{dR}{dr} \right) + \frac{2m_e r^2}{\hbar^2} \left(\frac{e^2}{4\pi\epsilon_0 r} + E \right) R(r) \right] = -\beta \quad (25)$$

and

$$-\frac{1}{Y(\theta, \phi)} \left[\frac{1}{\sin \theta} \frac{\partial}{\partial \theta} \left(\sin \theta \frac{\partial Y}{\partial \theta} \right) + \frac{1}{\sin^2 \theta} \frac{\partial^2 Y}{\partial \phi^2} \right] = \beta \quad (26)$$

We have incorporated \hbar^2 into our constant β . We can multiply Eq. 26 by the product of $\sin^2 \theta$ and $Y(\theta, \phi)$ to get

$$\sin \theta \frac{\partial}{\partial \theta} \left(\sin \theta \frac{\partial Y}{\partial \theta} \right) + \frac{\partial^2 Y}{\partial \phi^2} + (\beta \sin^2 \theta) Y = 0 \quad (27)$$

We consider the angular parts of the hydrogen atomic orbitals as rigid-rotator wave functions and the radial part of the hydrogen atomic orbitals as the solutions of the radial equation. We will solve the angular part first and then the radial part.

4.1.1 Separating the angular parts

In order to be able to solve Eq. 27 we will use the method of separation of variables, this time on the θ and ϕ terms by letting

$$Y(\theta, \phi) = \Theta(\theta)\Phi(\phi) \quad (28)$$

Substituting Eq. 28 into Eq. 27 and dividing by $\Theta(\theta)\Phi(\phi)$, we get

$$\frac{\sin \theta}{\Theta(\theta)} \frac{d}{d\theta} \left(\sin \theta \frac{d\Theta}{d\theta} \right) + \beta \sin^2 \theta = m^2 \quad (29)$$

and

$$\frac{1}{\Phi(\phi)} \frac{d^2\Phi}{d\phi^2} = -m^2 \quad (30)$$

where m^2 is the separation constant, we will use the square root of the separation constant later in the solution.

4.1.2 Solving the phi part

Because Eq.30 contains only constant coefficients, it is fairly easy to solve for,

$$\Phi(\phi) = A_{m_l} e^{im_l\phi} \text{ and } \Phi(\phi) = A_{-m_l} e^{-im_l\phi} \quad (31)$$

For one full rotation on the xy plane in one direction, the wave function must coincide with itself (be cyclic) so that,

$$\Phi(\phi + 2\pi) = \Phi(\phi) \quad (32)$$

Substituting Eq.32 into Eq.31 we see that,

$$A_{m_l} e^{im_l(\phi+2\pi)} = A_{m_l} e^{im_l\phi} \quad (33)$$

and

$$A_{-m_l} e^{-im_l(\phi+2\pi)} = A_{-m_l} e^{-im_l\phi} \quad (34)$$

These two equations together imply that

$$e^{\pm i2\pi m} = 1 \quad (35)$$

In terms of sines and cosines, we can rewrite Eq.35 as

$$\cos(2\pi m_l) \pm i \sin(2\pi m_l) = 1 \quad (36)$$

This only holds true for integer values of m_l which we refer to as the magnetic quantum number which we introduced earlier in this report.

$$m_l = 0, \pm 1, \pm 2, \dots$$

The unnormalized ϕ component to the angular wave function is then:

$$\boxed{\Phi(\phi) \propto e^{im_l\phi}}$$

4.1.3 Solving the theta part

The differential equation for $\Theta(\theta)$, Eq. 29 is not as easily solved due to its lack of constant coefficients. We can make this solution slightly simpler by letting $x = \cos \theta$ and $\Theta(\theta) = P(x)$ in Eq. 29. If $0 \leq \theta \leq \pi$ then the range of x is $-1 \leq x \leq +1$. Under the change of variables Eq. 29 becomes,

$$(1 - x^2) \frac{d^2 P}{dx^2} - 2x \frac{dP}{dx} + \left[\beta - \frac{m_l^2}{1 - x^2} \right] P(x) = 0 \quad (37)$$

When $m_l = 0, \pm 1, \pm 2, \dots$ Eq.37 for $P(x)$ is a well-known equation in classical physics called *Legendre's equation*. When Eq. 37 is solved, it is found that β must equal $l(l + 1)$ with $l = 0, 1, 2, \dots$ and that $|m| \leq l$, where $|m|$ denotes the magnitude of m . With finite solutions Eq. 37 can be written as

$$(1 - x^2) \frac{d^2 P}{dx^2} - 2x \frac{dP}{dx} + \left[l(l + 1) - \frac{m_l^2}{1 - x^2} \right] P(x) = 0 \quad (38)$$

with $l = 0, 1, 2, \dots$ and $m_l = 0, \pm 1, \pm 2, \dots, \pm l$

This equation is known as an *associated Legendre-type differential equation*, and has solutions known as the *associated Legendre polynomials*.

TABLE 2

The first few associated Legendre polynomials $P_l^{|m_l|}(x)$

$P_0^0(x) = 1$
$P_1^0(x) = x = \cos \theta$
$P_1^1(x) = (1 - x^2)^{1/2} = \sin \theta$
$P_2^0(x) = \frac{1}{2}(3x^2 - 1) = \frac{1}{2}(3 \cos^2 \theta - 1)$
$P_2^1(x) = 3x(1 - x^2)^{1/2} = 3 \cos \theta \sin \theta$
$P_2^2(x) = 3(1 - x^2) = 3 \sin^2 \theta$
$P_3^0(x) = \frac{1}{2}(5x^3 - 3x) = \frac{1}{2}(5 \cos^3 \theta - 3 \cos \theta)$
$P_3^1(x) = \frac{3}{2}(5x^2 - 1)(1 - x^2)^{1/2} = \frac{3}{2}(5 \cos^2 \theta - 1) \sin \theta$
$P_3^2(x) = 15x(1 - x^2) = 15 \cos \theta \sin^2 \theta$
$P_3^3(x) = 15(1 - x^2)^{3/2} = 15 \sin^3 \theta$

The solution to Eq.27 which contains both the angular and rigid-rotator wave functions of the hydrogen atomic orbitals is then $P_l^{|m_l|}(\cos \theta) \Phi_{m_l}(\phi)$. We construct the form of the unnormalized spherical harmonics $Y_l^{m_l}(\theta, \phi)$:

$$Y_l^{m_l}(\theta, \phi) \propto P_l^{|m_l|}(\cos \theta) e^{im_l \phi}$$

TABLE 3

The first few spherical harmonics

$Y_0^0 = \frac{1}{(4\pi)^{1/2}}$	$Y_1^0 = \left(\frac{3}{4\pi}\right)^{1/2} \cos \theta$
$Y_1^1 = \left(\frac{3}{8\pi}\right)^{1/2} \sin \theta e^{i\phi}$	$Y_1^{-1} = \left(\frac{3}{8\pi}\right)^{1/2} \sin \theta e^{-i\phi}$
$Y_2^0 = \left(\frac{5}{16\pi}\right)^{1/2} (3 \cos^2 \theta - 1)$	$Y_2^1 = \left(\frac{15}{8\pi}\right)^{1/2} \sin \theta \cos \theta e^{i\phi}$
$Y_2^{-1} = \left(\frac{15}{8\pi}\right)^{1/2} \sin \theta \cos \theta e^{-i\phi}$	$Y_2^2 = \left(\frac{15}{32\pi}\right)^{1/2} \sin^2 \theta e^{2i\phi}$
$P_2^{-2} = \left(\frac{15}{32\pi}\right)^{1/2} \sin^2 \theta e^{-2i\phi}$	

4.1.4 Solving the radial part

Eq. 25 with β set equal to $l(l+1)$ can be written as

$$-\frac{\hbar^2}{2m_e r^2} \frac{d}{dr} \left(r^2 \frac{dR}{dr} \right) + \left[\frac{\hbar^2 l(l+1)}{2m_e r^2} - \frac{e^2}{4\pi\epsilon_0 r} - E \right] R(r) = 0 \quad (39)$$

Eq. 39 is an ordinary differential equation in r . It is somewhat tedious to solve, but once solved we find that in order for solutions to be acceptable as the wave functions, the energy must be quantised according to

$$E_n = -\frac{e^2}{8\pi\epsilon_0 a_0 n^2} \quad n = 1, 2, \dots \quad (40)$$

These are the same energies obtained from the Bohr model of the hydrogen atom, however the electron is not restricted to the defined Bohr orbits but instead is described by its wave function, $\psi(r, \theta, \phi)$.

In Eq. 39 $R(r)$ takes an unnormalized form, which uses the *associated Laguerre polynomials* $L_{n+1}^{2l+1} \left(\frac{2r}{na_0} \right)$ as a function of the principal quantum number n and radial position r .

$$R_{nl}(r) = - \left\{ \frac{(n_l - 1)!}{2n[(n+l)!]^3} \right\}^{1/2} \left(\frac{2}{na_0} \right)^{l+3/2} r^l e^{-r/na_0} L_{n+l}^{2l+1} \left(\frac{2r}{na_0} \right) \quad (41)$$

The first few associated Laguerre polynomials are given below

TABLE 4

The first few associated Laguerre polynomials.

$n = 1$	$l = 0$	$L_1^1(x) = -1$
$n = 2$	$l = 0$	$L_2^1(x) = -2!(2 - x)$
	$l = 1$	$L_3^3(x) = -3!$
$n = 3$	$l = 0$	$L_3^1(x) = -3!(3 - 3x + \frac{1}{2}x^2)$
	$l = 1$	$L_4^3(x) = -4!(4 - x)$
	$l = 2$	$L_5^5(x) = -5!$
$n = 4$	$l = 0$	$L_4^1(x) = -4!(4 - 6x + 2x^2 - \frac{1}{6}x^3)$
	$l = 1$	$L_5^3(x) = -5!(10 - 5x + \frac{1}{2}x^2)$
	$l = 2$	$L_6^5(x) = -6!(6 - x)$
	$l = 3$	$L_7^7(x) = -7!$

4.1.5 Putting together the full wave function

Finally we arrive at the wave function

$$\psi(r, \theta, \phi) = R_{nl}(r)Y_l^{m_l}(\theta, \phi) \quad (42)$$

We now know the form of the hydrogen atom wave functions. We will list the normalised wave functions for the ground state $n = 1$ and first excited state $n = 2$ of the hydrogen atom

TABLE 5The complete hydrogenlike atomic wave functions for $n = 1$ and 2.

$n = 1$	$l = 0$	$m = 0$	$\psi_{100} = \frac{1}{\sqrt{\pi}} \left(\frac{Z}{a_0}\right)^{3/2} e^{-\sigma}$
$n = 2$	$l = 0$	$m = 0$	$\psi_{200} = \frac{1}{\sqrt{32\pi}} \left(\frac{Z}{a_0}\right)^{3/2} (2 - \sigma)e^{-\sigma/2}$
	$l = 1$	$m = 0$	$\psi_{210} = \frac{1}{\sqrt{32\pi}} \left(\frac{Z}{a_0}\right)^{3/2} (\sigma)e^{-\sigma/2} \cos \theta$
	$l = 1$	$m = \pm 1$	$\psi_{21\pm 1} = \frac{1}{\sqrt{64\pi}} \left(\frac{Z}{a_0}\right)^{3/2} (\sigma)e^{-\sigma/2} \sin \theta e^{\pm i\phi}$

Finally, if we want to find the energy of the ground state atomic orbital wave function ψ_{100} , we evaluate the triple integral in all space:

$$E = \int_0^{2\pi} \int_0^\pi \int_0^\infty \psi_{100}^*(r, \theta, \phi) \hat{H} \psi_{100}(r, \theta, \phi) r^2 dr \sin \theta d\theta d\phi \quad (43)$$

In atomic units, the ground-state energy for the hydrogen atom is -0.5000 Hartrees, or -13.61 eV.

4.2 Using the Hartree-Fock Method to Calculate Water

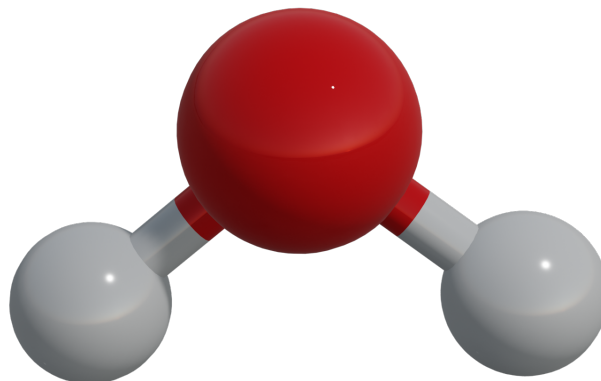


Figure 7: Rendered image of a H₂O Molecule

As a first example, the Hartree-Fock method calculates a relatively small molecule of water. We started off by performing a geometry optimisation, changing the systems nuclear coordinates to minimise the total energy of the system. This was followed by a tight geometry optimisation which is the same process but with a tighter convergence criteria for the total energy of the system.

We performed a benchmarking of different basis sets which we can compare with accepted known values for H₂O since it is such a well studied molecule, the basis sets included in the benchmarking are def2-TZVP, STO-3G and TZVP. The results are as follows

TABLE 6

Benchmarking results of H₂O using the Hartree-Fock Method 2.2

Basis set	Ground state energy (Hartrees)	NIST Database (Hartrees)
def2-TZVP	-75.7403285841	-76.063178
STO-3G	-74.6426504733	-74.965901
TZVP	-75.7392828032	-76.056800

From the table we can see all of the ground state energies of H₂O against a value obtained from the NIST database^[35], STO-3G performs the worst with the largest discrepancy being -0.3232505267 Hartrees or $\sim 0.43\%$. The most accurate basis set is TZVP with a discrepancy of -0.3175171968 Hartrees or $\sim 0.41\%$.

We also obtained Vibrational Frequency data for the H₂O molecule which we can compare against the NIST database and also plot as an IR Spectrum.

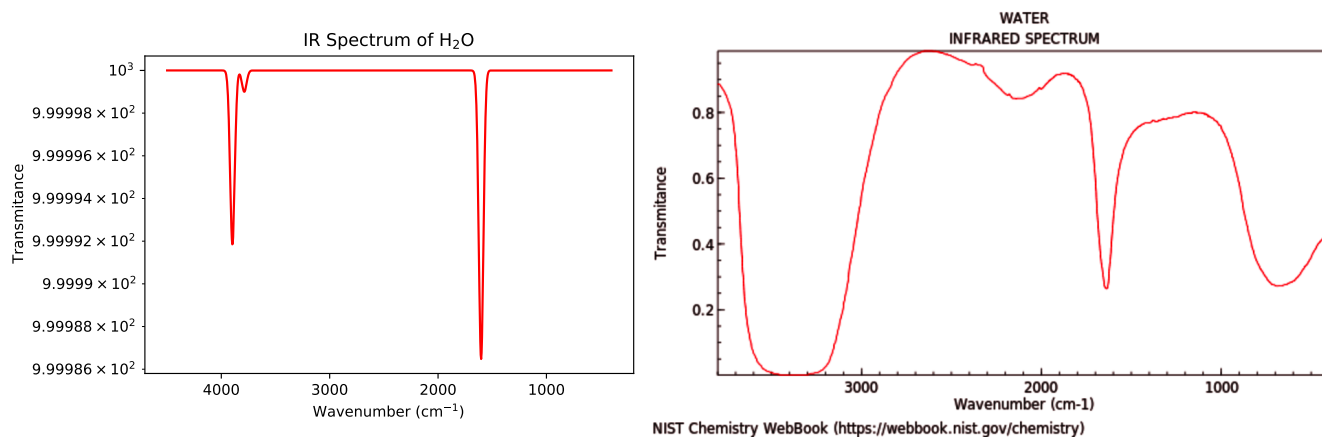


Figure 8: Comparison between H₂O IR spectrum and NIST database^[33]

The IR Spectrum for Water was generated using the TZVP basis set and shows three distinct peaks. We can associate these peaks with the three vibrational modes of water. Water is a non-linear molecule and therefore the number of vibrational modes can be calculated using

$$3(N) - 6 = \text{Number of vibrational modes} \quad (44)$$

Where N is the number of atoms in the molecule

Therefore the number of vibrational modes in H₂O is:

$$3(3) - 6 = 3$$

These vibrational modes correspond to one bending mode, one symmetrical stretch and one asymmetrical stretch of the water molecule.

TABLE 7

Calculated Vibrational modes of H₂O - comparison With NIST database^[34]

Vibrational Mode	Calculated Frequency (cm ⁻¹)	NIST Frequency (cm ⁻¹)
Symmetrical stretch	3788	3832
Bending	1603	1649
Asymmetrical stretch	3897	3943

For the symmetrical stretch we got a discrepancy of 44 cm⁻¹ or ~1%, for the bending mode we got a discrepancy of 46 cm⁻¹ or ~3% and for the asymmetrical stretch we got a discrepancy of 46 cm⁻¹ or ~1%. From the benchmarking we carried out TZVP was quantitatively the best basis set to use when attempting to calculate H₂O and gave us the best comparison with values found in the NIST Database^[34].

4.3 Using the Hartree-Fock Method to Calculate Benzene

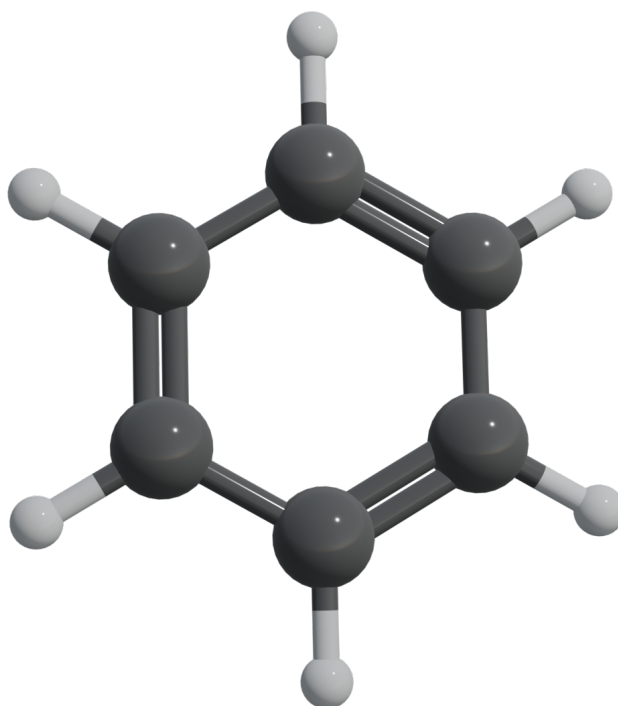


Figure 9: Rendered image of a benzene molecule

The next example is what is considered to be a relatively large molecule in terms of Hartree-Fock calculations but a relatively small molecule in chemistry terms. Benzene has a chemical formula of C_6H_6 and has 42 electrons in total. This is a large molecule when you consider that each electron is included in a 42×42 Slater determinant and has to pass through the Fock operator. Despite the attempts to approximate the electron-electron repulsion term as an average and discounting two electron integral terms that are zero or near zero, for molecules like benzene this still leaves a huge number of non-zero two electron integrals which must be solved. In fact from the information provided from the output file of our Hartree-Fock calculation

```
TOTAL NUMBER OF NONZERO TWO-ELECTRON INTEGRALS =          1957454
      131 INTEGRAL RECORDS WERE STORED ON DISK FILE  8.
..... END OF TWO-ELECTRON INTEGRALS .....
```

Figure 10: Two-electron integrals section of HF output file

for Benzene we can see that there are a total of 1,957,454 nonzero two-electron integrals that must be solved. This harkens back to the theory section on the Hartree-Fock method when we stated that two-electron repulsion integrals are almost always the most expensive step of integral-direct self consistent field methods.

We performed a benchmarking of different basis sets which we can compare with accepted known values for C_6H_6 and attempt to find the optimal basis set for our calculations, the basis sets included in the benchmarking are def2-TZVP, STO-3G and TZVP. The results are as follows

TABLE 8Benchmarking results of C_6H_6 using Hartree-Fock Method 2.2

Basis set	Ground state energy (Hartrees)	NIST Database (Hartrees)
def2-TZVP	-230.785284879646	-230.787450
STO-3G	-227.891359694036	-227.891360
TZVP	-230.68645	-230.773604

From the table we can see all of the ground state energies of C_6H_6 against a value obtained from the NIST database, STO-3G performs the best with the smallest discrepancy being -0.000000305963 Hartrees or $\sim 0.43\%$. The least accurate basis set is TZVP with a discrepancy of -0.087154 Hartrees or $\sim 0.41\%$. It is always important to choose the right basis set for the particular molecule you are working with, in our previous example H_2O TZVP performed the best and STO-3G performed the worst however in the case of C_6H_6 the reverse is true.

We also obtained Vibrational Frequency data for the C_6H_6 molecule which we can compare against the NIST database and also plot as an IR Spectrum.

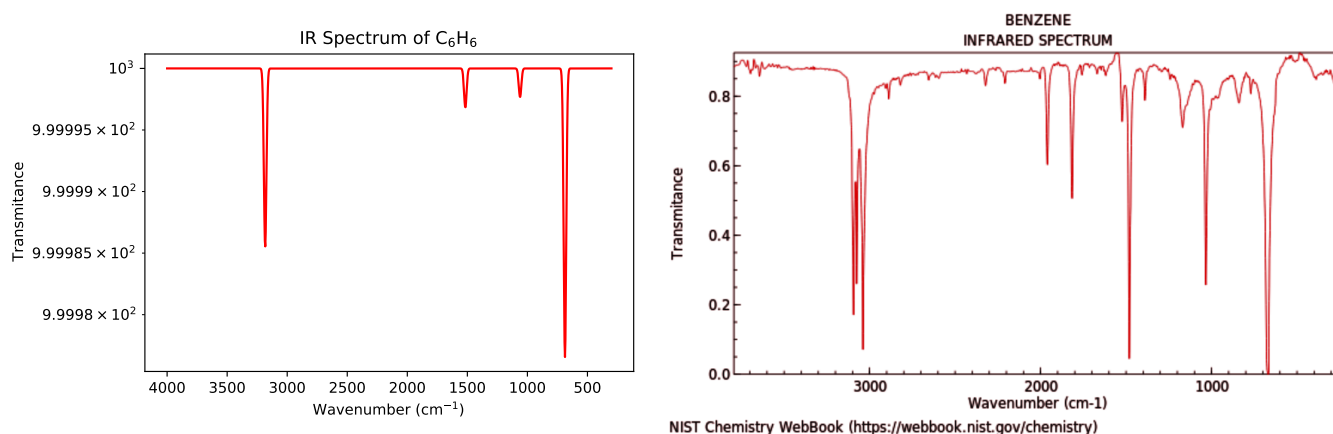


Figure 11: Comparison between C_6H_6 IR Spectrum Hartree-Fock Methods 2.2 and NIST Database

The IR Spectrum for Benzene was generated using the STO-3G basis set and shows four distinct peaks. We can associate these peaks with the three vibrational modes of water. Benzene is a non-linear molecule and therefore the number of vibrational modes can be calculated using Eq. 42 the number of vibrational modes in C_6H_6 is:

$$3(12) - 6 = 30$$

Despite only four distinct peaks being visible our output file does contain 30 different vibrational frequencies however only four have intensities great enough to be visible, these occur at 687 cm^{-1} , 1059.53 cm^{-1} , 1515.25 cm^{-1} , 3182.60 cm^{-1} . These values correspond to the known IR active modes of Benzene^[36]

TABLE 9Calculated Vibrational modes of C₆H₆ - comparison With NIST database^[37]

Vibrational Mode	Calculated Frequency (cm ⁻¹)	NIST Frequency (cm ⁻¹)
A _{2u}	687	673
E _{1u}	1059.53	1038
E _{1u}	1515.25	1486
E _{1u}	3182.60	3063

For the A_{2u} vibrational mode we got a discrepancy of 14 cm⁻¹ or ~2%, for the first E_{1u} vibrational mode we got a discrepancy of 22 cm⁻¹ or ~2%, from the second E_{1u} vibrational mode we got a discrepancy of 29 cm⁻¹ or ~2% and from the last E_{1u} vibrational mode we got a discrepancy of 120 cm⁻¹ or ~4%. From the benchmarking we carried out STO-3G was quantitatively the best basis set to use when attempting to calculate C₆H₆ and gave us the best comparison with values found in the NIST Database^[37].

4.4 Using Density Functional Theory to Calculate Pyrene

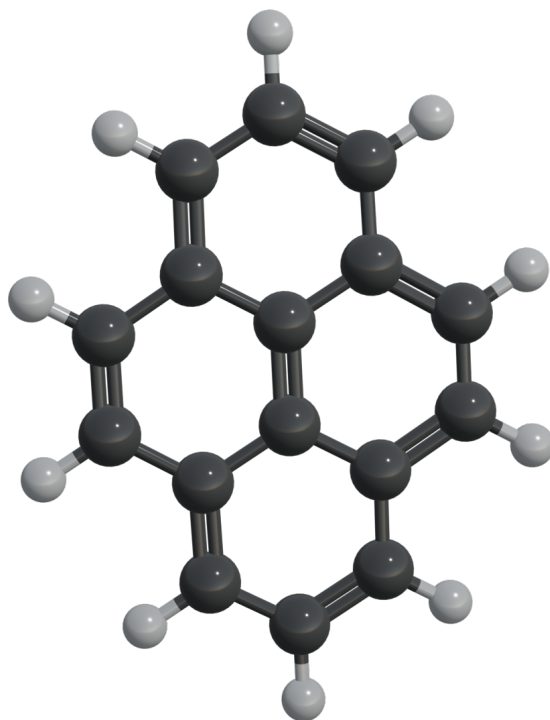


Figure 12: Rendered image of a pyrene molecule

An obvious progression from calculating Benzene is to perform a calculation on another acene molecule. Acenes are hydrocarbons made up of benzene rings which are linearly fused. Pyrene is a polycyclic aromatic hydrocarbon consisting of four fused benzene rings with a chemical formula of $C_{16}H_{10}$.

Once again we used B3LYP as our functional and performed a benchmarking test with our basis sets.

TABLE 10

Benchmarking results of $C_{16}H_{10}$ using Density Functional Theory 2.3

Basis set	Ground state energy (Hartrees)	NIST Database (Hartrees)
STO-3G	-608.242387	-608.242393
LanL2DZ	-615.6761297	-615.676125
SDD	-615.6766539	-615.676649

For the STO-3G basis set we got a discrepancy of $6 \times 10^{-7} \text{ cm}^{-1}$ or $\sim 9.86 \times 10^{-7} \%$, for the LanL2DZ basis set we got a discrepancy of $4.7 \times 10^{-7} \text{ cm}^{-1}$ or $\sim 7.63 \times 10^{-7} \%$ and the SDD basis set gave us a discrepancy of $4.9 \times 10^{-7} \text{ cm}^{-1}$ or $\sim 7.96 \times 10^{-7} \%$. Moving forward with calculations of Pyrene in DFT we will use the LanL2DZ basis set as it gives us the closest values to NIST database values^[38].

We generate a UV/VIS spectrum of Pyrene in its gas form in order to be able to compare our computationally obtained spectrum with an experimental UV/VIS spectrum found in the literature.

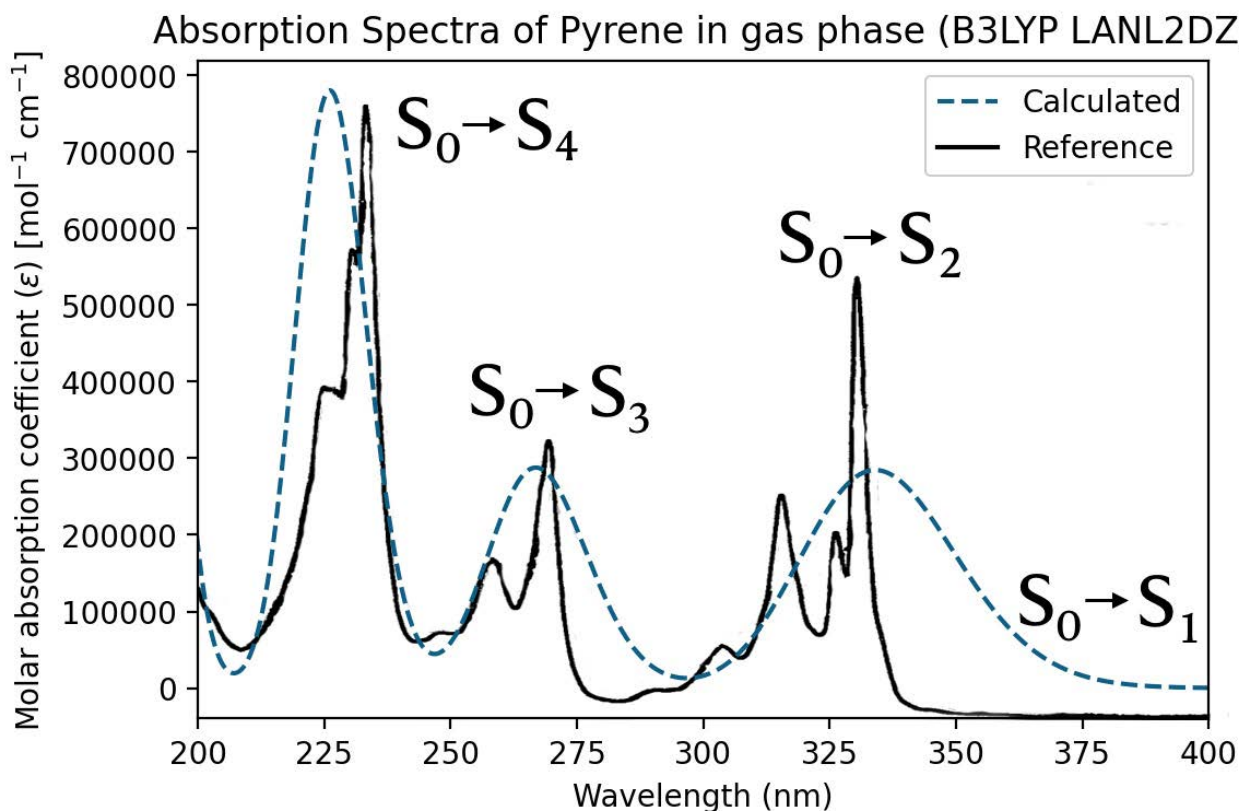


Figure 13: Computed Pyrene UV/VIS spectrum compared to the spectrum reported by Thony et al.^[39]

In Fig.11 we see a strong similarity between both the calculated spectrum and reference spectrum. Both of the graphs contain 3 transitions at roughly the same wavelength ranges around 225 nm, 260 nm and 340 nm. These transitions can be mapped to $S_0 \rightarrow S_4$, $S_0 \rightarrow S_3$, $S_0 \rightarrow S_2$ and a forbidden $S_0 \rightarrow S_1$ transition^[40] due to symmetry which is not present in either spectrum. These transitions match those found within the literature.^[41]

An attempt was made at producing a UV/VIS spectrum for pyrene in its liquid phase for various solvents such as acetonitrile and acetone as it is well reported in the literature that Pyrene in its liquid phase has an absorption peak in the visible part of the spectrum around 480 nm.^[42] We were unable to obtain this transition regardless of solvent used, this is most likely due to the fact that our current dft model only accounts for a single Pyrene molecule and this absorption peak is the result of pyrene forming an excimer when two molecules of pyrene interact with each other.^[43]

The possibility of pi stacking pyrene molecules within the initial dft input file could potentially resolve this issue however, in the interest of time it was not explored in this report.

4.5 Using Density Functional Theory to Calculate Tris(bipyridine) Ruthenium(II) Chloride

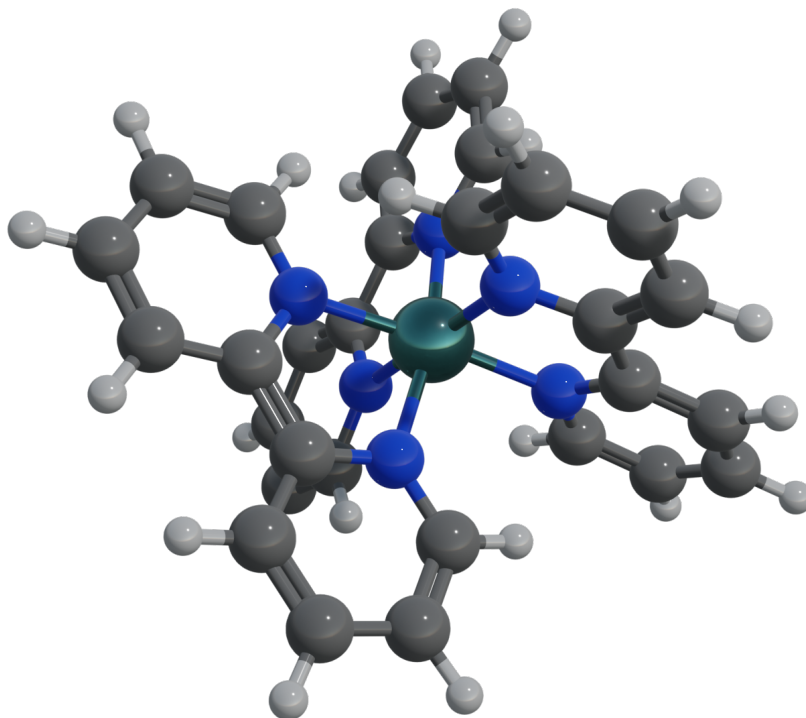


Figure 14: Rendered image of a tris(bipyridine) ruthenium(II) chloride molecule

Before collecting results for Tris(bipyridine) Ruthenium(II) Chloride which has the chemical formula $C_{30}H_{24}N_6Cl_2Ru \cdot 6H_2O$ the decision was made to switch from the B3LYP functional to using the CAM-B3LYP function. CAM stands for Coulomb-attenuation method, the functional attempts to combine the benefits of the B3LYP hybrid function while also improving long range correction, this was shown to improve the performance of charge transfer excitations^[44] which will be crucially important in our characterisation of this molecule.

There is no Hartree energy data in the NIST database regarding this molecule so we will just have to work on information we have gathered thus far and assume that the LanL2DZ is the most optimal basis set for this molecule as it has been for the previous two molecules.

We will once again compare our calculated UV/VIS spectrum against one found in the literature for our particular molecule. The UV/VIS spectrum of Tris(bipyridine) Ruthenium(II) Chloride was generated in liquid phase using acetonitrile as the solvent to match the one found in the literature.

The UV/VIS data is included below

Absorption Spectra of Ru(BPY)3 in water (CAM-B3LYP LANL2DZ)

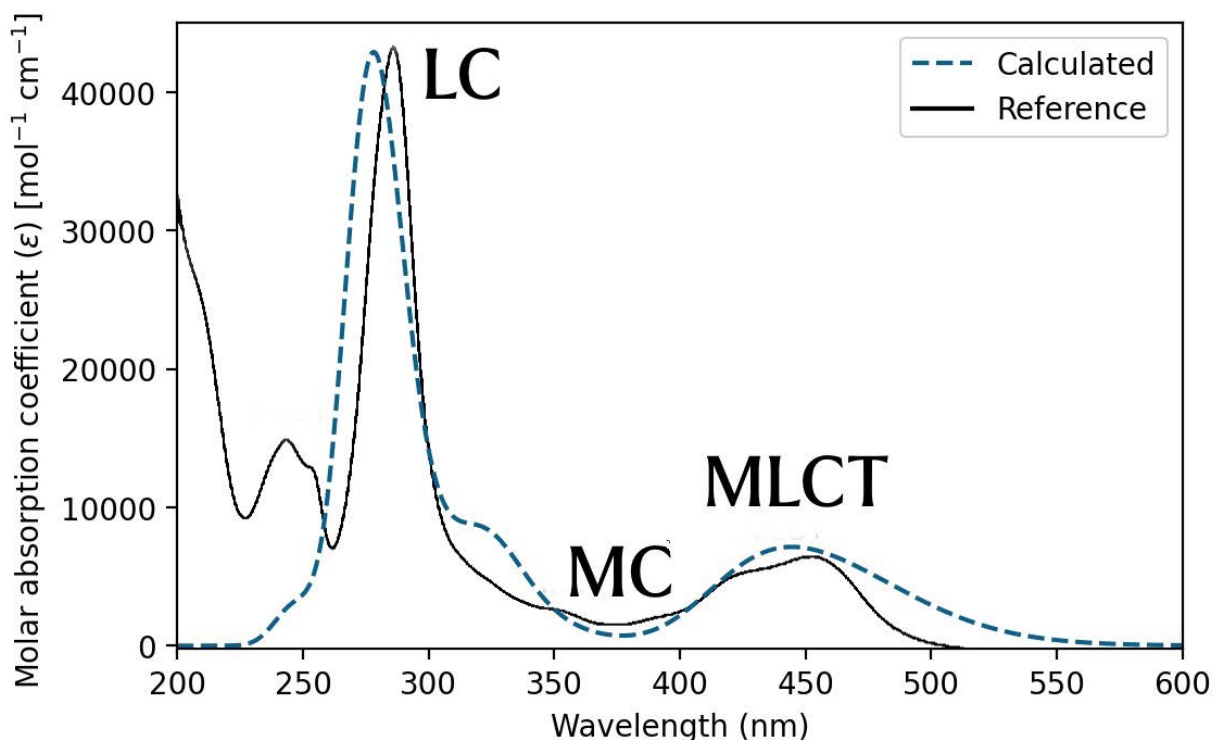


Figure 15: Computed Tris(bipyridine) Ruthenium(II) Chloride UV/VIS spectrum compared to the spectrum reported by Filevich et al.^[45]

We can clearly see 3 distinct transitions in Fig. 13 with the strongest peak at 280 nm being associated to a Ligand Centred (LC) transition, when the electrons are transferred from the pi-bonding orbital to the anti-bonding orbital of the ligand ($\pi \rightarrow \pi^*$).

The second peak occurs at 360 nm and is associated with a Metal Centred (MC) transition and occurs as a result of weak electron transfer inside the transition metal due to a splitting of the d-orbitals of the central ruthenium atom, the electron transfers from the lower to the higher level ($t_{2g} \rightarrow e_g$). Since our molecule is centrosymmetric, transitions between subshells are actually forbidden under the Laporte Rule. Typically when we see these weak MC transitions in experimental data we attribute them to vibronic coupling, however in the case of our calculated data vibronic coupling is neglected under the Born-Oppenheimer approximation and therefore we believe we are seeing the MC transition as a result of mixing of the d and pi orbitals.

Finally we see a Metal to Ligand Charge Transfer (MLCT) at 450 nm this occurs when electrons in the metal-centered t_{2g} orbital are promoted into the ligand-centered π^* orbital, in our case electrons are transferred from the ruthenium core to one of the bipyridine ligands. This absorption at 450 nm gives the aqueous solution of Ru(BPY)₃ its distinctive orange colour. The MLCT is also interesting because it excites from a singlet state to a triplet state by way of InterSystem Crossing (ISC), triplet states are electronic states whereby two electrons in different molecular orbitals have parallel spins. Singlet-triplet transitions are forbidden and often slow.

5 Conclusion

Laser-Induced Dynamics was successfully modelled using the Hartree-Fock method on simple molecules such as H₂O which produced vibrational mode frequencies which were within ~3 % of the expected values found within the NIST database. We also successfully managed to model laser-induced dynamics in benzene, a resist material which gave vibrational mode frequencies within ~4 % of the expected values found in the NIST database. Density Functional Theory was successfully used to produce a UV-Vis spectrum of Pyrene in the gas phase which could be compared with a similar graph found in the literature from an experimental measurement. Both graphs showed three transitions which we were able to label as $S_0 \rightarrow S_4$, $S_0 \rightarrow S_3$ and $S_0 \rightarrow S_2$ transitions, both graphs did not have the $S_0 \rightarrow S_1$ transition which is expected as this transition is forbidden due to symmetry. Pyrene also has a strong absorption peak at 480 nm in liquid phase which we were unable to replicate due to our calculations not accounting for excimer behaviour which results from Pyrene molecules interacting with each other. This opens the door for further exploring methods of inducing excimer behaviour in the future including the proposed pi stacking method of setting up the initial DFT file. Finally we were able to use Density Functional Theory to successfully produce a UV-Vis spectrum of Tris(bipyridine) Ruthenium(II) Chloride in aqueous solution which could be compared with a similar graph found in the literature from an experimental measurement. Both graphs had matching transitions at 280 nm, 360 nm and 450 nm, these were characterised as a Ligand Centred ($\pi \rightarrow \pi^*$) transition, Metal Centred ($t_{2g} \rightarrow e_g$) and Metal-to-Ligand Charge Transfer ($t_{2g} \rightarrow \pi^*$) respectively.

References

- [1] G. E. Eyre and W. Spottiswoode. Specifications of alphonse louis poitevin photographic engraving. *The Great Seal Patent Office*, pages 1–6, April 1856.
- [2] R. H. Marjorie Devon, Bill Lagattuta. Tamarind techniques for fine art lithography. *Abrams*, pages 183–201, 2009.
- [3] J. Nall and J. Lathrop. Photolithographic fabrication techniques for transistors which are an integral part of a printed circuit. In *1957 International Electron Devices Meeting*, pages 117–117, 1957.
- [4] J. R. N. Jay W. Lathrop. Semiconductor construction. *U.S. Patent 2,890,395*, October 31 1957 and granted June 9, 1959.
- [5] G.-D. Mélanie, D. Georges, R. Emmanuel, and A. Nadir. 10 - balloon-borne and airborne measurements. In W. Chen, D. S. Venables, and M. W. Sigrist, editors, *Advances in Spectroscopic Monitoring of the Atmosphere*, pages 521–601. Elsevier, 2021.
- [6] S. A. Benjamin, F. F. Hahn, B. E. Powers, and D. F. Kusewitt. 22 - radiation and heat. In W. M. HASCHEK, C. G. ROUSSEAUX, and M. A. WALLIG, editors, *Handbook of Toxicologic Pathology (Second Edition)*, pages 529–594. Academic Press, San Diego, second edition edition, 2002.
- [7] B. Bahreyni. Chapter 2 - microfabrication. In B. Bahreyni, editor, *Fabrication and Design of Resonant Microdevices*, Micro and Nano Technologies, pages 9–46. William Andrew Publishing, Norwich, NY, 2009.
- [8] C. K. Ober, V. Kosma, H. Xu, K. Sakai, and E. P. Giannelis. The challenges of highly sensitive euv photoresists. *Journal of Photopolymer Science and Technology*, 31(2):261–265, 2018.
- [9] A. Vaglio Pret, E. Kunnen, R. Gronheid, E. Pargon, O. Luere, and D. Bianchi. 2d and 3d photoresist line roughness characterization. *Microelectronic Engineering*, 110:100–107, 2013.
- [10] B. MOLLOY. Swords and swordsmanship in the aegean bronze age. *American Journal of Archaeology*, 114(3):403–428, 2010.
- [11] M. M. A. Hendriksen. Criticizing chrysopoeia? alchemy, chemistry, academics, and satire in the northern netherlands, 1650–1750. *Isis*, 109(2):235–253, 2018.
- [12] F. Habashi. The age of alchemy history of chemistry, metallurgy, and civilisation. *Interdisciplinary Science Reviews*, 23(4):348–361, 1998.
- [13] G. B. Kauffman. *Classics in Coordination Chemistry, Part 1: The Selected Papers of Alfred Werner*. Dover Publications, 1968.
- [14] J. E. House and K. A. House. Chapter 2 - atomic structure and properties. In J. E. House and K. A. House, editors, *Descriptive Inorganic Chemistry (Third Edition)*, pages 11–22. Academic Press, Boston, third edition edition, 2016.
- [15] J. C. Slater. The self consistent field and the structure of atoms. *Phys. Rev.*, 32:339–348, Sep 1928.

- [16] J. C. Slater. Note on hartree’s method. *Phys. Rev.*, 35:210–211, Jan 1930.
- [17] F. V. Selfconsistent field mit austausch fur natrium. *Zeitschrift fur Physik*, 62(11):795–805, November 1930.
- [18] W. Heisenberg. Mehrkörperproblem und resonanz in der quantenmechanik. *Zeitschrift für Physik*, 38(6):411–426, 1926.
- [19] P. A. M. Dirac and R. H. Fowler. On the theory of quantum mechanics. *Proceedings of the Royal Society of London. Series A, Containing Papers of a Mathematical and Physical Character*, 112(762), 1926.
- [20] L. Goletto, E. F. Kjønstad, S. D. Folkestad, I.-M. Høyvik, and H. Koch. Linear-scaling implementation of multilevel hartree–fock theory. *Journal of Chemical Theory and Computation*, 17(12):7416–7427, 2021. PMID: 34747179.
- [21] K. G. Johnson, S. Mirchandaney, E. Hoag, A. Heirich, A. Aiken, and T. J. Martínez. Multinode multi-gpu two-electron integrals: Code generation using the regent language. *Journal of Chemical Theory and Computation*, 18(11):6522–6536, 2022. PMID: 36200649.
- [22] C. C. J. Roothaan. New developments in molecular orbital theory. *Rev. Mod. Phys.*, 23:69–89, Apr 1951.
- [23] T. H. Kim. An iterative technique for solving the n -electron hamiltonian: The hartree-fock method. 2008.
- [24] D. A. D. A. McQuarrie. *Physical chemistry : a molecular approach*. Sausalito, Calif. : University Science Books, [1997] ©1997, [1997].
- [25] M. Head-Gordon, R. J. Rico, M. Oumi, and T. J. Lee. A doubles correction to electronic excited states from configuration interaction in the space of single substitutions. *Chemical Physics Letters*, 219(1):21–29, 1994.
- [26] G. D. Purvis and R. J. Bartlett. A full coupled cluster singles and doubles model the inclusion of disconnected triples. *The Journal of Chemical Physics*, 76(4):1910–1918, 1982.
- [27] H.-D. Meyer, U. Manthe, and L. Cederbaum. The multi-configurational time-dependent hartree approach. *Chemical Physics Letters*, 165(1):73–78, 1990.
- [28] K. Burke. Perspective on density functional theory. *The Journal of Chemical Physics*, 136(15):150901, 2012.
- [29] S. Kurth, M. Marques, and E. Gross. Density-functional theory. In F. Bassani, G. L. Liedl, and P. Wyder, editors, *Encyclopedia of Condensed Matter Physics*, pages 395–402. Elsevier, Oxford, 2005.
- [30] H. J. Jang, S. L. Hopkins, M. A. Siegler, and S. Bonnet. Frontier orbitals of photosubstitutionally active ruthenium complexes: an experimental study of the spectator ligands’ electronic properties influence on photoreactivity. *Dalton Trans*, 46:9969–9980, 2017.
- [31] G. L. Miessler, P. J. Fischer, and D. A. Tarr. *Inorganic chemistry*. Pearson advanced chemistry series. Pearson, Boston, fifth edition edition, 2014.
- [32] F. Neese, F. Wennmohs, U. Becker, and C. Riplinger. The orca quantum chemistry program package. *The Journal of Chemical Physics*, 152(22):224108, 2020.

- [33] N. I. of Standards and Technology. NIST Chemistry WebBook, SRD 69, Water.
- [34] N. I. of Standards and Technology. Computational chemistry comparison and benchmark database - experimental data for h₂o (water).
- [35] N. I. of Standards and Technology. Computational chemistry comparison and benchmark database - energies for h₂o (water).
- [36] W. J. Huang, A. Azizi, T. Xu, S. R. Kirk, and S. Jenkins. A vector-based representation of the chemical bond for the normal modes of benzene. *International Journal of Quantum Chemistry*, 118(19), 2018.
- [37] N. I. of Standards and Technology. Computational chemistry comparison and benchmark database - experimental data for c₆h₆ (benzene).
- [38] N. I. of Standards and Technology. Computational chemistry comparison and benchmark database - energies for c₆h₁₀ (pyrene).
- [39] A. Thöny and M. J. Rossi. Gas-phase uv spectroscopy of anthracene, xanthone, pyrene, 1-bromopyrene and 1,2,4-trichlorobenzene at elevated temperatures. *Journal of Photochemistry and Photobiology A: Chemistry*, 104(1):25–33, 1997.
- [40] H. Bettermann. The quantitative determination of the s₀ - t₁ absorption in pyrene with the use of intracavity absorption spectroscopy. *Spectrochimica Acta Part A: Molecular Spectroscopy*, 50(6):1073–1079, 1994.
- [41] J. Merz, J. Fink, A. Friedrich, I. Krummenacher, H. H. A. Mamari, S. Lorenzen, M. Haehnel, A. Eichhorn, M. Moos, M. Holzapfel, H. Braunschweig, C. Lambert, A. Steffen, L. Ji, and T. B. Marder. The multi-configurational time-dependent hartree approach. *Chemical Physics Letters*, 165(1):73–78, 1990.
- [42] C. R. Goldschmidt and M. Ottolenghi. Absorption spectrum of the pyrene excimer. *The Journal of Physical Chemistry*, 74(9):2041–2042, 1970.
- [43] G. K. Bains, S. H. Kim, E. J. Sorin, and V. Narayanaswami. The extent of pyrene excimer fluorescence emission is a reflector of distance and flexibility: Analysis of the segment linking the ldl receptor-binding and tetramerization domains of apolipoprotein e3. *Biochemistry*, 51(31):6207–6219, 2012. PMID: 22779734.
- [44] T. Yanai, D. P. Tew, and N. C. Handy. A new hybrid exchange–correlation functional using the coulomb-attenuating method (cam-b3lyp). *Chemical Physics Letters*, 393(1):51–57, 2004.
- [45] O. Filevich, L. Zayat, L. M. Baraldo, and R. Etchenique. *Long Wavelength Phototriggering: Ruthenium-Based Caged Compounds*, pages 47–68. Springer Berlin Heidelberg, Berlin, Heidelberg, 2015.

Associated Risk List

Student Name:	Jamie Somers
Student Number:	19330931
Project Title:	Simulating Laser-Induced Dynamics in Next Generation Photo-Acid Materials for EUVL
Main Project Working Location:	School of Physical Science, DCU
Supervisor Name:	Prof. John Costello and Dr. Lazaros Varvarezos
Brief Listing of All Risks Associated with Project (bullet point format):	
Computational Project. <ol style="list-style-type: none">1. Eye Strain2. Carpel Tunnel Syndrome3. Repetitive Stain Injury4. Tendonitis	

Signature page

Student:

I have attempted, to the best of my ability, to assess the risks associated with my project and to suggest appropriate controls and other measures to reduce the risk level. I have also consulted with my supervisor in performing and completing this risk assessment. I will implement these controls and other measures to reduce the risk level consistently throughout my project and make my supervisor aware if at any stage I feel the current risk assessment is insufficient as the project evolves*.

Student Name: Jamie Somers

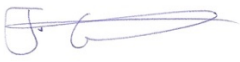
Student number: 19330931

Signature: Submission of this document is equivalent to a signature.

Date: 17/11/2022

Supervisor:

I confirm that the student has undertaken a risk assessment of their project work and that they have consulted with me on this matter. Furthermore, the assessment above appears thorough and I will inform the student if at any stage I feel the current risk assessment is insufficient as the project evolves**.

Supervisor Name:  and 

Signature: Submission of this document is contingent upon supervisor's approval and implies it has been sort and approved.

Date: 17/11/2022

**The implementation of controls will be monitored throughout the year by Dr. Paul Swift and Mr. Patrick Wogan.*

***This risk assessment document should be revised by the student in the early part of semester 2, and a brief discussion of this should form part of the mid-term meeting on progress at that stage.*